

Author's Response

1

2 We thank the 2 anonymous reviewers and John Dykema for their very useful comments and
3 suggestions for the paper. In our individualised replies, we have addressed each of the
4 reviewer's comments separately and made the relevant changes to the manuscript where
5 necessary. Below, we amalgamate the individual responses and changes to the manuscript,
6 and then provide a revised manuscript. Note that significant changes have been made to the
7 Supplement, including the addition of Section 2 – describing our method for conducting the
8 simulations.

9 Sections

10	p1-12	Response to Anonymous Referee #1
11	p13-22	Response to Anonymous Referee #2
12	p22	Response to John Dykema
13	p23-64	Revised Manuscript

14

15 Anonymous Referee #1

16 1. Abstract - The reviewer notes that the following statement is too strong:

17 *As injection rates for titania are close to those for sulfate, there appears to be little*
18 *benefit of using titania when compared to the injection of sulfur dioxide*

19 In response, we amend the statement to the following:

20 *As injection rates and climatic impacts for titania are close to those for sulfate,*
21 *there appears to be little benefit in terms of climatic influence of using titania*
22 *when compared to the injection of sulfur dioxide*

23 The amended statement takes into account that the conclusion is relevant with respect
24 to the climatic impacts of titania and sulfate injection.

25

26 2. Introduction – The reviewer questions why we chose RCP8.5 as a baseline scenario.

27 We have explained why we chose RCP8.5 in the following sentence, which is on
28 P30046.

29 *RCP8.5 is selected to give a significant greenhouse effect against which to employ*
30 *geoengineering, in order to distinguish the climatic impacts specific to each aerosol*

1 We appreciate however that the choice of RCP8.5 over the more societally-optimistic
2 RCP4.5 scenario is slightly-controversial (and novel) and will affect the findings of
3 this report. In particular, the aerosol injection rates, deposition rates, mass
4 concentrations and the magnitude of stratospheric changes would all be different with
5 a baseline RCP4.5 scenario. We modify the introduction as follows.

6 *RCP8.5, which is the high-end carbon-intensive CMIP5 scenario, is selected to*
7 *give a significant greenhouse effect against which to employ geoengineering, in order*
8 *to distinguish the climatic impacts specific to each aerosol. Observations have shown*
9 *that the current global GHG emissions exceed the emissions inherent in RCP8.5*
10 *[Peters et al, 2013]; therefore our work could be considered as geoengineering against*
11 *a business-as-usual scenario. Additionally, the next generation of GeoMIP*
12 *simulations (GeoMIP6) will utilise a carbon-intensive scenario [Kravitz et al, 2015],*
13 *hence our work will provide a useful supplement to those results.*

14 Also, in section 5, we have added the following paragraph to discuss the possible
15 differences if RCP4.5 had been used.

16 *The climatic impacts described in section 4 are specific to geoengineering*
17 *against a baseline RCP8.5 scenario. If instead we had used a middle-of-the-road*
18 *GHG-concentrations scenario such as RCP4.5 [Taylor et al., 2012], as used in*
19 *the first tier of GeoMIP scenarios [Kravitz et al., 2011], then less aerosol-*
20 *injection would be needed to obtain TOA-Imb=0 and therefore the aerosol*
21 *deposition rates and atmospheric mass concentrations would be less than those*
22 *reported in section 4. One would expect that the magnitude of stratospheric*
23 *temperature changes (fig. 8) and therefore zonal-mean zonal wind changes (fig.*
24 *12) would be much less for each of the aerosols, possibly confounding the*
25 *conclusions giving here relating to their comparative efficacy. An estimate for the*
26 *amount of SAI required for RCP4.5 can be garnered from integrating the*
27 *temperature anomalies for RCP8.5 and RCP4.5 for the period 2020-2100. The*
28 *ratio of the integrated temperature anomalies for RCP4.5 to RCP8.5 is 0.43,*
29 *hence we can assume that the injection rates required for RCP4.5 are ~0.43 of*
30 *those for RCP8.5, producing a climate perturbation ~0.43 times as great. A*
31 *further set of simulations, which instead utilise RCP4.5 as the baseline scenario,*
32 *would be required to test this hypothesis.*

33

1 3. Figure 1 – The reviewer questions the discontinuities between the short wave and
2 long wave points in figure 1. The discontinuities between the short wave and long
3 wave points in figure 1 are not due to uncertainty in the optical properties. Rather, the
4 wavelength at which the points are plotted is the average wavelength of the spectral
5 waveband used in the model. There are 5 disparate wavebands in the short wave
6 spectrum and 9 wavebands in the long wave. In the short wave, the wavebands used
7 for this experiment are 0.2-0.32, 0.32-0.69, 0.69-1.19, 1.19-2.38, and 2.38-10 μm . In
8 the long wave, the wavebands used are 3.34-6.67, 6.67-7.52, 7.52-8.33, 8.93-10.1,
9 8.33-12.5, 13.3-16.9, 12.5-18.1, 18.1-25, 25-10000 μm . It is then clear that the
10 average-wavelengths of the wavebands of the two spectrums overlap (max SW = 6.19
11 μm , min LW = 5 μm), which explains the disparity in figure 1. The equivalent image
12 from Ferraro et al (2011) – their figure 1 – shows the same discontinuities between
13 the short wave and long wave bands, which is because both our models (their FDH
14 code, our HadGEM2-CCS) use the Edwards and Slingo radiation code (ES96) and we
15 both evaluate the optical constants at the same wavebands [Edwards and Slingo,
16 1996]. We appreciate that this point was not made clear in the article and could cause
17 confusion to a reader. Therefore we amend the caption in figure 1 as follows.

18 *“Figure 1. Optical properties as a function of wavelength for a) accumulation-mode
19 sulfate, b) titania, c) black carbon. Points are plotted at the
20 middle of each spectral waveband, as detailed in Bellouin et al (2007)”*

21
22 4. Figure 1 & figure 10 – The reviewer questions why we get different results to Ferraro
23 et al (2011). There are many differences between the models and configurations used
24 by ourselves and Ferraro et al (2011), hereafter F11, which could contribute to the
25 different stratospheric temperature perturbations. We will concentrate on sulfate and
26 titania, as black carbon is similar between the two, and give possible reasons for the
27 temperature-change differences. We will then summarise these for addition to the
28 article.

- 29 a. The first point is that F11 use a fixed dynamical heating (FDH) code and not a
30 dynamical-model; their code doesn't take into account feedback from changes
31 in the atmospheric and oceanic circulation, sea surface temperatures, etc as
32 HadGEM2-CCS will. Also their model has 38 vertical levels up to 40 km
33 altitude rather than the 60 vertical levels up to 85 km in our model

- 1 b. The second point is that we use inherently different climatologies, which
2 include different ozone, baseline stratospheric temperatures, greenhouse gases,
3 clouds, etc. All of which will contribute to the overall temperature change
- 4 c. The third point is that we use different size distributions for titania and sulfate.
5 We chose the titania size distribution ($r_m=0.045 \mu\text{m}$, $\sigma=1.8$) from considering
6 results of Pope et al (2012), namely that this is an optimised size distribution
7 for a scattering aerosol. F11's size distribution ($r_m=0.1 \mu\text{m}$, $\sigma=2.0$) was
8 selected from observations of natural mineral dust aerosols of which titania is
9 a minor component. The key difference between these size distributions is the
10 median radius, which is much smaller in our case, and therefore the titania
11 aerosols in our simulations absorb and scatter short wave radiation more
12 efficiently, hence more solar radiation is absorbed in the aerosol layer
13 resulting in greater stratospheric heating.
- 14 For sulfate, we took the *volc2* size distribution from Rasch et al (2008)
15 ($r_m=0.376 \mu\text{m}$, $\sigma=1.25$) which is based on stratospheric aerosol observations in
16 a post-volcanic period. Our Pinatubo simulations in section 3 show close
17 conformity to observations. F11's sulfate size distribution ($r_m=0.1 \mu\text{m}$, $\sigma=2.0$)
18 is much wider (i.e. their σ is greater). Therefore, while the effective radii of
19 the distributions are comparable (0.43 and 0.33 respectively), F11 has more
20 coarse particles that absorb efficiently in the long wave spectrum. Hence F11's
21 sulfate has a greater stratospheric heating efficacy (i.e. heating per burden)
22 than our sulfate, from more long wave absorption
- 23 d. The fourth point is that our aerosol layer is much higher than F11's idealised
24 aerosol layer. Whereas our aerosol concentrations peak at ~30 km altitude,
25 F11's are evenly spaced between the tropopause and 22km altitude. Again, we
26 have the advantage of accurate dynamical transport as we are using a 3-D
27 global model
- 28 e. For titania, F11 use the parallel refractive indices, from Ribarsky (1977) whilst
29 we use an average of the parallel and perpendicular (or ordinary and
30 extraordinary – denoting the polarisation of the scattered field). Angus Ferraro
31 (personal communication) reports that, when re-running their FDH code with
32 the perpendicular refractive indices instead of parallel, “the perpendicular
33 refractive indices produce slightly stronger tropical heating”
- 34

1 Although points (a), (b), (d), and (e) will contribute to the difference in stratospheric
2 temperatures (i.e. that our titania produces more warming, whilst their sulfate
3 produces more warming), it is point (c) that is likely most important. We believe that
4 our chosen size-distributions are appropriate for the study here, as Pope et al (2012)
5 try and maximise the impact of a specifically tailored TiO₂ aerosol. We therefore add
6 the following paragraph to the discussion.

7 *We find that sulfate induces less stratospheric warming than titania. In contrast,*
8 *Ferraro et al (2011) found that the peak stratospheric warming for titania was 30%*
9 *of that from sulfate. Although the different climatologies, model configurations, and*
10 *aerosol spatial distributions will contribute to the difference in stratospheric*
11 *temperature adjustment between our and Ferraro's work, the primary reason for the*
12 *disparity is likely to be the aerosol size distributions. Our titania is smaller (median*
13 *radius = 0.045 μm compared to 0.1 μm for Ferraro et al (2011)) and therefore*
14 *scatters and absorbs SW more efficiently, producing a greater localised 'solar'*
15 *warming. Their sulfate distribution contains a larger spread ($\sigma = 2.0$ for Ferraro et al*
16 *(2011) compared to $\sigma = 1.25$ here), resulting in more coarse-mode particles and*
17 *greater LW absorption. This disparity further highlights the sensitivity of climatic*
18 *effects to the specified aerosol size distribution.*

19 While we are comparing our work with Ferraro et al (2011), it is necessary to
20 highlight major errors within their work that should be taken into account when
21 comparing our results. In a personal communication, Angus Ferraro informed me that
22 the aerosol density was not modified/ considered in either the calculation of the
23 optical properties or the specification of the aerosol layer mass in their work. This is
24 important - the specific absorption/ scattering coefficients plotted in their figure 1 are
25 intrinsic properties; they depend on the density of the aerosol. The assumed density of
26 1000 kg/m³ as used by Ferraro et al (2011) for calculation of all their aerosol's optical
27 properties is not appropriate for either sulfate or titania, which should be represented
28 by densities of ~1600 kg/m³ and ~4000 kg/m³. Consequently, the coefficients plotted
29 for sulfate and titania in their figure 1 should be multiplied by 1/1.6 and 1/4
30 respectively to obtain realistic values. Similarly, the mass burdens given in their table
31 1 for sulfate and titania should be multiplied by 1.6 and 4 respectively to obtain
32 appropriate values. This correction gives forcing efficiencies comparable to ours (see
33 the table below). Should the disparity between the optical coefficients in our figure 1

1 and theirs be scrutinised, then this is the explanation. We have added the following to
2 the above paragraph.

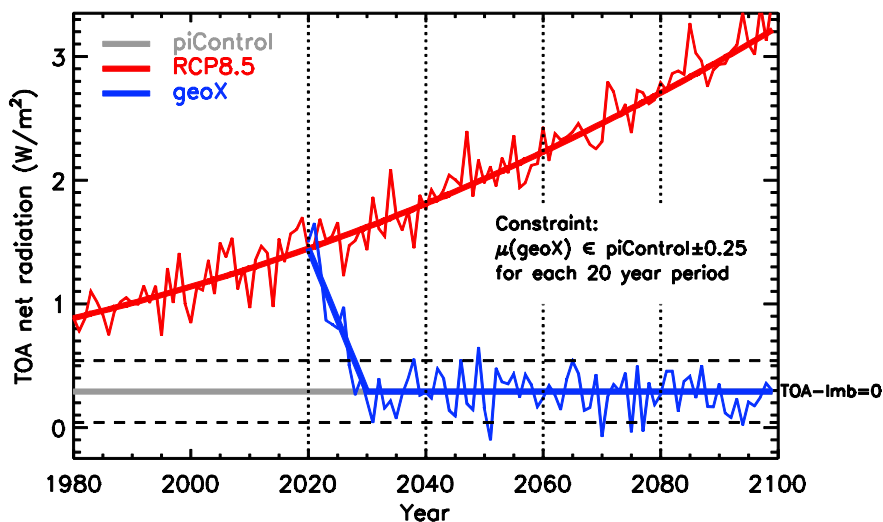
3 *On a separate note, Ferraro et al (2011) neglected to alter the aerosol density*
4 *component in the calculation of their aerosol masses and specific optical*
5 *properties [A. Ferraro, personal communication]. The density that they used for*
6 *all the aerosols of 1000 kg/m³ is arguably applicable to black carbon, but not to*
7 *sulfate and titania (which instead are ~1600 and ~4000 kg/m³). Therefore, their*
8 *aerosol burdens for sulfate and titania should be multiplied by 1.6 and 4*
9 *respectively, and their optical coefficients divided by 1.6 and 4, to obtain*
10 *appropriate values.*

Table T1	Sulfate		Titania	
	F11	This work	F11	This work
Burden (Tg)	14.5	49.5	3	20.2
Estimated Forcing (Wm ⁻²)	3.5	8.5	3.5	8.5
Forcing efficiency (Wm ⁻² Tg ⁻¹)	0.24	0.17	1.17	0.42
Corrected burden (Tg)	23.2	49.5	12	20.2
Corrected forcing efficiency (Wm ⁻² Tg ⁻¹)	0.15	0.17	0.29	0.42

11

12 5. P30050 – The reviewer notes that the description we provide for our methods is
13 insufficient. We appreciate that this aspect of the report is under-developed and would
14 benefit from further detail. We therefore describe the exact methods used to obtain
15 injection rates and conduct the simulations, in order that a reader would be able to
16 reproduce these results.
17

1 Firstly, as noted by another reviewer, the top of the atmosphere radiative flux
 2 imbalance (hereafter *TOA-Imb*) is loosely defined in the report and requires further
 3 elaboration. To calculate the TOA-Imb for a certain simulation, we calculate the TOA
 4 net radiation (incoming SW minus outgoing LW+SW) and average this annually and
 5 globally (denote this value $R(t)$ where t refers to the year). Next we do the same for
 6 each year of the 240-year perpetual pre-industrial control simulation. We then average
 7 these values to obtain the net radiative imbalance of the pre-industrial control
 8 simulation (denote this C). The TOA-Imb for year t is calculated as $R(t) - C$. The
 9 following has been added to the supplement to explain the method.



10 **Fig. S2** Schematic of the geoengineering experiment outline

11
 12
 13
 14
 15
 16
 17
 18
 19
 20
 21

We now describe the simulation timeline. The RCP8.5 simulations had already been conducted prior to this investigation. The geoengineering simulations took place in 3 distinct phases: (a) we performed atmosphere-only simulations of 1Tg/yr aerosol injection to determine the aerosol TOA radiative effect; (b) we used the aerosol radiative effect to calculate initial injection rate estimates; (c) we began the 80-year GCM integrations, calibrating the injection rates *en route*.

- 1 a. We performed atmosphere-only simulations with a constant 1 Tg/yr aerosol
 2 injection rate using historical background-conditions (1990-2005). We then
 3 determined the steady-state annual/global-mean aerosol radiative effect (the
 4 difference in TOA net radiation between the aerosol simulation and the
 5 control), which is given in the following table. For sulfate, because the
 6 radiative effect was small, we performed an additional simulation with
 7 5Tg[SO₂]/yr and then divided the results by 5 for precision. Similarly, the

Table T2	Sulfate	Titania	Black Carbon
TOA radiative effect (Wm ⁻² / Tg yr ⁻¹)	0.46	1.1	7.4

8 black carbon simulation failed to converge to steady state within 15 years and
 9 was therefore run for a further 15 years.

10

- 11 b. Rather than use the TOA-Imb from the RCP8.5 simulations to estimate the
 12 required aerosol injection rates, we instead used the Anthropogenic Radiative
 13 Forcing (ARF), which was acquired from [http://www.pik-
 14 potsdam.de/~mmalte/rcps/](http://www.pik-potsdam.de/~mmalte/rcps/) (see Meinshausen et al, 2011). Specifically, we
 15 deducted the 1860 ARF (0.17 Wm⁻²) from the ARFs for 2020, 2040, 2060,
 16 2080, and 2100, and then calculated the injection rates required to offset these
 17 adjusted ARFs by dividing by the TOA aerosol radiative effect. Because each
 18 model will have an ARF which is different from Meinshausen et al (2011) it is
 19 possible that our initial estimate is in error. However, our method uses this
 20 only as an initial 1st guess for the injection rates, which are iteratively adjusted
 21 as described in c). The model then linearly interpolates the injection rates
 22 between these years.

Table T3	Anthro-RF (Wm ⁻²)		SO ₂ injection rate (Tg/yr)		Titania injection rate (Tg/yr)		BC injection rate (Tg/yr)	
	Actual	Adjusted	Initial	Final	Initial	Final	Initial	Final
Year								
2020	2.56	2.39	5.2	4.4	2.2	1.4	0.32	0.21
2040	3.83	3.66	8.0	7.4	3.3	2.5	0.49	0.29

2060	5.34	5.17	11.2	11.6	4.7	4.1	0.70	0.45
2080	6.79	6.62	14.4	13.6	6.0	4.8	0.89	0.62
2100	8.15	7.98	17.4	14.2	7.3	6.2	1.08	0.88

1
2 c. A single simulation was then initiated for each aerosol, with initial injection
3 rates as specified in table T3. After every 20 year interval, the simulation was
4 stopped and the TOA-Imb was calculated for that time period. If there was
5 significant deviation from zero (we adopted $|\text{mean}(\text{TOA-Imb})| > 0.25 \text{ Wm}^{-2}$ as
6 the criterion), then we recalculated the amount of injection required. The
7 recalibration was conducted as follows: the TOA-RF at the end of the 20 year
8 period (time = t_{20}) was calculated for the mean of the RCP8.5 ensemble,
9 denote this R_{rcp} . The injection of aerosol at time t_{20} at rate I_{geo} produced TOA-
10 Imb R_{geo} which we wish to be zero. Therefore an improved injection rate at t_{20}
11 would be $I'_{geo} = I_{geo} R_{rcp} / (R_{rcp} - R_{geo})$. Additionally, at all specified timesteps
12 after t_{20} ($t_n = t_{20} + 20n$, $n = 1, \dots$), we modify the injection rate as such: $I'_{geo}(t_n) =$
13 $I_{geo}(t_n) R_{rcp} / (R_{rcp} - R_{geo})$. After resetting the injection rates, we restarted the
14 simulation from the start of the last time period. Final injection rates are given
15 in table T3. We then used the final injection rates to run two more ensemble
16 members for each aerosol
17

18 We agree with the reviewer that it is important to include all of this information in our
19 work so that our results are readily reproducible; therefore we have added this to the
20 supplementary material. We will also the following sentence to section 3, to point the
21 reader to the supplementary material for a detailed methodology.

22 *A detailed description of our methods is provided in the supplementary material*
23 *(section S2).*

24 We add the following to our Methods section.

25 *We inject aerosol at such a rate as to maintain the top-of-the-atmosphere (TOA)*
26 *net radiation at piControl levels. Specifically, we define the TOA radiative flux*
27 *Imbalance (TOA-Imb) as the annual/global-mean TOA net radiation (incoming*
28 *SW minus outgoing LW+SW) minus the average TOA net radiation of the*
29

1 *piControl period. By sufficient aerosol injection, we aim to maintain TOA -Imb=0.*
2 *This scenario represents our interpretation of 'equal amount of geoengineering'*
3 *for each aerosol. The advantage of returning net radiation to piControl levels*
4 *(rather than completely equilibrating TOA fluxes) is that piControl had already*
5 *been simulated comprehensively for CMIP5 (240 model-years), hence permitting*
6 *robust statistics to be calculated. The TOA radiative imbalance is a metric that*
7 *satellites are able to measure (e.g. CERES [L'Ecuyer et al, 2015] and EarthCare*
8 *[Illingworth et al, 2015]), albeit with +/- 3 W/m² accuracy at present [Priestley*
9 *et al, 2011; von Schuckmann et al., 2016]. Therefore our target could be*
10 *applicable to an actual SAI scenario. In contrast, Radiative Forcing (RF) (the net*
11 *radiation perturbation at the tropopause from some external forcing, after*
12 *stratospheric adjustment), cannot be directly measured by satellites and therefore*
13 *it would be difficult to obtain a specified radiative forcing in an actual SAI*
14 *scenario. Of course, other metrics could be chosen [e.g. MacMartin et al., 2013],*
15 *with each metric having its only signal/noise characteristic.*

- 16
17 6. P30057 – The reviewer notes that our analysis pertaining to the hydrological cycle is
18 too inadequate. We have altered the sentences concerning the hydrological cycle to
19 add clarity to our argument.

20 *Additionally, producing an equivalent top of the atmosphere radiative perturbation*
21 *with a SW-absorbing aerosol such as BC (or to a lesser extent titania) compared to a*
22 *SW-scattering aerosol such as sulfate, induces a comparatively greater SW forcing at*
23 *the surface. Bala et al (2008) showed that reduced latent heat fluxes compensate for*
24 *the SW reduction at the surface, instigating a deceleration of the hydrological cycle*
25 *that is proportional to the magnitude of the SW reduction. This explains the greater*
26 *reduction in precipitation exhibited by BC in figures 6-8.*

- 27
28 7. P30058 – This query forms two separate parts: (a) what is the likelihood of the BC
29 and titania aerosol being/ becoming hygroscopic? (b) And would this impact the
30 results given here? We assess these questions and summarise our findings for addition
31 to the manuscript.

- 32
33 a. Firstly, for this analysis we will assume that mineral dust represents titania as
34 this is the most apposite natural proxy [Ndour et al, 2008]. Mineral dust

1 consists of 1-10% titania by mass depending on location [Ndour et al, 2008]
2 and therefore is arguably suitable for this approximation. The chemical and
3 physical attributes of atmospheric (or at least tropospheric) BC are
4 comparatively well-known [Liu et al, 2013]. Koehler et al (2009) show that
5 most atmospheric mineral dust exhibits low hygroscopicity ($\kappa \sim 0.03$)
6 although larger particles ($r_m > 0.1 \mu\text{m}$) exhibit a similar hygroscopicity to
7 similar sized sea-salt and ammonium sulfate aerosols. Liu et al (2013) show
8 that atmospheric BC generally exhibits low hygroscopicity in its pure form (g_F
9 ~ 1.05) but the inclusion of soluble contaminants such as secondary organics
10 increases the hygroscopicity ($g_F \sim 1.25$). Therefore, fresh BC and titania
11 particles are likely to exhibit low hygroscopicity and cloud condensation
12 activity, but in an aged form and when internally mixed with hygroscopic
13 species their hygroscopic activity will increase.

- 14 b. We apply the hygroscopic growth scheme used for sulfate [d' Almeida et al,
15 1991] to titania and BC, using the same size-distributions and properties as
16 used in the article, in order to test the sensitivity of the optical properties to
17 hygroscopicity. The 550nm absorption and scattering coefficients for BC are
18 approximately similar for dry aerosol and at $< 30\%$ Relative Humidity (RH),
19 but increase by 10% and 40% respectively at 50% RH. For titania, the 550 nm
20 absorption and scattering coefficients are also similar for dry mode and at
21 $< 30\%$ RH, but increase by 55% and 32% respectively at 50% RH.

22
23 To summarise, the hygroscopicity of the BC and titania aerosol would increase over
24 time due to internal mixing with hygroscopic constituents and coagulation, the latter
25 process resulting in larger particles that can act as cloud condensation nuclei (CCN).
26 However, the low relative humidity of the stratosphere ($\sim 0.3\%$ [SPARC, 2006])
27 would result in minimal hygroscopic growth, and therefore our results should not be
28 significantly affected.

29 *Observations have shown that fresh BC aerosol is predominantly hydrophobic,*
30 *but the uptake of soluble contaminants (e.g. secondary organics) results in*
31 *increased hygroscopicity [Liu et al, 2013]. Mineral dust, which contains 1-10%*
32 *titania by mass [Ndour et al, 2008], exhibits low hygroscopicity for radii < 0.1*
33 *μm and similar growth to equivalently-sized sulfate aerosol thereafter [Koehler*
34 *et al, 2009]. Although the historical stratospheric water vapor content is low*

1 *(~4.2 ppmv in the tropical lower stratosphere during the HIST period), aerosol-*
2 *induced stratospheric warming in the TTL would increase the specific humidity of*
3 *air entering the stratosphere, therefore impacting hygroscopic growth.*
4

- 5 8. P30059 – Thanks for the comment, we have added the Tang et al reference to this
6 section.

7 *This work has already been started for titania by Tang et al [2014].*
8

- 9 9. P30059 – We agree with the reviewer that this section is under-developed and with
10 questionable applicability. The NIOSH recommendations refer to particles less than
11 radius < 0.05 μm as ‘ultrafine’ and < 1.5 μm as ‘fine’. For titania, NIOSH
12 recommends time-weighted-average exposure limits of 0.3 mg/m^3 and 2.4 mg/m^3
13 respectively, allowing for a 10 hour day and 40 hour week. It is highly unlikely that
14 titania injected in the ultrafine mode in the stratosphere will remain in the ultrafine
15 mode until deposition. Therefore, we add the second NIOSH exposure
16 recommendation for fine particles and a caveat.

17 *... the USA’s National Institute for Occupational Safety and Health (NIOSH)*
18 *recommends maximum exposure limits of 0.3 mg m^{-3} for ultrafine titania particles*
19 *(radius <0.05 μm) and 2.4 mg m^{-3} for fine particles (radius < 1.5 μm) [Dankovic et*
20 *al, 2011]. After undergoing coagulation and ageing in the atmosphere, it is likely that*
21 *the second exposure limit is more applicable to this work. In our simulations, the*
22 *maximum 2090’s near-surface air concentration of titania (e.g. Fig. 4) for land*
23 *regions between 60°S-60°N is 254 ng/m^3 , which is of the order of 10^2 less than the*
24 *NIOSH ‘fine-particle’ exposure limit.*
25

- 26 10. P30048 – The reviewer notes that the units for the scattering/absorption coefficients
27 are incorrect. Thanks for the comment - the units have been corrected.

- 28
29 11. P30052 – The reviewer suggests that we add the titania deposition rate (the sulfate
30 and BC deposition rates are already given). Thanks for the comment, the TiO_2
31 deposition rate has been added (11 $\text{mg}/\text{m}^2/\text{yr}$).
32
33

1 **Anonymous Reviewer #2**

2

3 1. The reviewer notes that the acronym ‘RF’ is used for both anthropogenic *radiative*
4 *forcing* (ARF) and top-of-the-atmosphere *radiative flux imbalance* (TOA-RF).

5 Radiative forcing and radiative fluxes are different concepts; therefore the use of RF
6 for both might confuse a reader. We therefore use the acronym *TOA-Imb* instead of
7 *TOA-RF*.

8

9 2. The reviewer highlights that the GeoMIP ‘G3’ specifications are significantly
10 different from our specifications, both in the baseline GHG-concentrations scenario
11 (we use RCP8.5, GeoMIP uses RCP4.5) and in goals (we target TOA radiative fluxes,
12 GeoMIP targets radiative forcing). Therefore the reviewer recommends that we use a
13 different nomenclature for our geoengineering simulations, which we agree to.
14 Therefore *G3S*, *G3TiO₂* and *G3BC* are changed to *geoSulf*, *geoTiO₂*, and *geoBC*.

15

16 3. The reviewer questions the goal of the investigation; what does “maintain TOA-Imb
17 balance” entail? The reviewer also queries how the TOA-Imb relates to the radiative
18 forcing. We provide the following text in the Methods section, but also include an
19 entirely new section S2 in the Supplementary Material in which we describe how the
20 simulations were conducted. *See response 6 to Anonymous Referee #1*

21

22 4. The reviewer notes that the IPCC report citations concerning temperature trends are
23 only applicable to *radiative forcing* and not *radiative fluxes*. The reviewer questions
24 whether the temperature trends in fig. 3 are instead related to the consistently non-
25 adjusted stratosphere. The reviewer notes that the surface temperature disparities
26 might occur for an equal tropopause radiative forcing, if energy is distributed
27 differently in the climate system. In answer to these questions, we have assessed the
28 net radiative fluxes at the top of the atmosphere and the tropopause, and the net heat
29 flux (radiation + sensible + latent) at the surface. We firstly remove this analysis from
30 section 4.1:

31 *This is due to the absorption of radiation by BC (and a lesser extent the absorption by*
32 *titania) heating the stratosphere which then increases the terrestrial longwave*
33 *radiation entering the troposphere reducing the tropopause-RF. As noted in several*

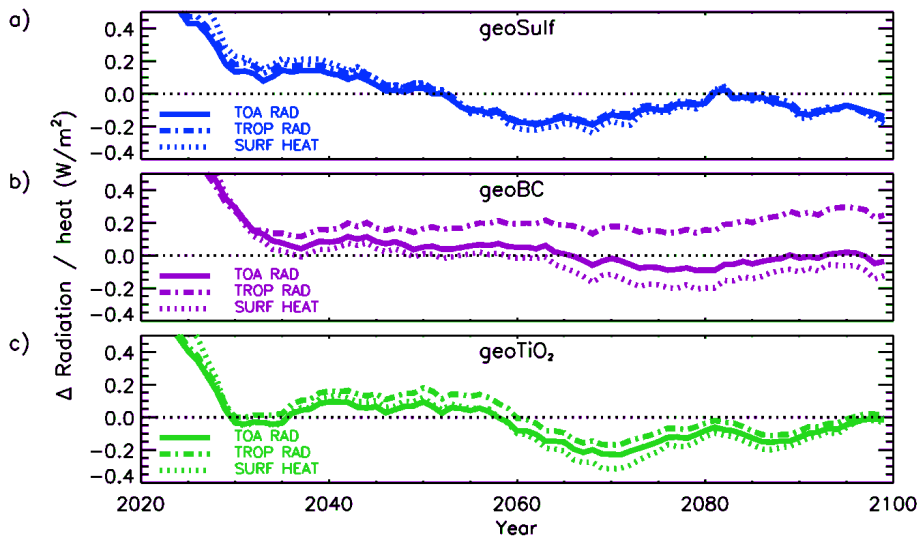
1 *Intergovernmental Panel on Climate Change reports [e.g. Ramaswamy et al., 2001;*
2 *Forster et al., 2007], it is the global mean tropopause-RF rather than the TOA-RFI*
3 *that is proportional to global mean surface temperature changes. Further analysis of*
4 *stratospheric temperature changes will be provided in section 4.4.*

5

6 The following is added in its place.

7 *The near-surface global temperature response differs between the aerosols with a*
8 *greater cooling trend for sulfate than for titania or BC (Fig. 3b). To determine*
9 *the cause of the anomalous warming in geoBC, we assess the net energy fluxes at*
10 *the top of the atmosphere for 2020-2100. Fig. S3 in the Supplement shows the*
11 *global-mean net-downward radiation anomaly for the geoengineering*
12 *experiments, evaluated at the TOA and the tropopause; and the global-mean net-*
13 *downward heat flux anomaly at the surface. The radiation changes at the TOA*
14 *and tropopause, and the heat flux anomaly at the surface, are comparable for the*
15 *geoSulf and geoTiO₂ experiments for the duration of 2020-2100. In contrast,*
16 *geoBC exhibits an increasingly positive net radiation anomaly at the tropopause*
17 *(+0.2 W/m² averaged over 2020-2100) despite the negligible TOA radiation*
18 *anomaly. After stratospheric temperature adjustment, radiative perturbations at*
19 *the TOA and tropopause are equal for a given climate forcing, which implies that*
20 *the consistently non-adjusted stratosphere (due primarily to increasing aerosol*
21 *injection rates) is responsible for the differences in TOA and tropopause*
22 *radiative perturbations in geoBC. This implies that if we had injected aerosol*
23 *sufficiently to produce an equal radiative effect at the tropopause, the*
24 *temperature trends for the geoengineering experiments in Fig. 3 would have been*
25 *more comparable. If we were to choose stabilisation of temperature as our basic*
26 *metric, then one could approximate the results by simply scaling the results by the*
27 *ratio of the temperature perturbation relative to 1980-2005 to that for geoSulf. The*
28 *scaling would be 1 (by design) for geoSulf, 1.1 for geoTiO₂ and 1.28 for geoBC. If the*
29 *metric chosen were instead to keep the global mean precipitation the same, then the*
30 *scaling would be 1 (by design) for geoSulf, 0.91 geoTiO₂ and 0.68 for geoBC.*
31 *However, we shall see that the changes in many of the variables we consider are*
32 *dominated by large scale changes in the spatial patterns of response rather than the*

1 *10-30% changes in magnitude of the response that applying such a scaling would*
 2 *induce. We therefore choose to present un-scaled results here but caveat that such a*
 3 *scaling could be applied should we wish to apply a different metric.*



4
 5 **Fig. S3** *10-year running-average global/annual-mean net radiation anomaly at*
 6 *the tropopause and TOA, and net-downward heat flux anomaly at the surface, with*
 7 *respect to piControl. Positive values indicate an increase in net downward flux.*

8
 9 a. The reviewer questions where the additional energy into the climate system in
 10 the geoSulf experiment goes, considering that temperatures decrease over time
 11 despite a net flux of energy into the system. Additionally the reviewer asks
 12 whether energy is conserved in the model. HadGEM2-CCS's dynamical core,
 13 'New-Dynamics', does not conserve energy [Davies et al., 2005]. Instead, an
 14 energy correction flux is applied at the end of each model day as a globally
 15 homogeneous heating-rate perturbation at all levels and grid-points. However,
 16 the fact that the temperature trend in fig. 3b is negative for geoSulf is more
 17 likely due to an uneven vertical distribution of this energy gain. The following
 18 explanation is added to the text.

19 *From Fig. 3b, geoSulf exhibits a near-surface air cooling trend with respect to*
 20 *2020 despite a net gain of atmospheric energy, which is likely due to an*
 21 *uneven vertical distribution of this energy gain.*

- 1 5. HIST period – The reviewer questions the motivations behind our choice of control
2 period (HIST: 1980-2005) and how this relates to the goal of our experiment. We
3 accept that our choice of control period is arbitrary, we chose this period as the
4 temperature change for geoSulf was approximately 0. We add the following
5 explanation for the choice of HIST period to the text.
6 *As we were not explicitly attempting to reach a specific global mean temperature,*
7 *the choice of reference period was left until after the geoengineering simulations*
8 *had been completed. We then selected a recent historical period from which the*
9 *2090s global-mean temperature anomaly for geoSulf was negligible (fig. 3b). The*
10 *HIST period selected is close to the historical control period used in the IPCC*
11 *AR5 report (1860-2005) [e.g. Fig. 12.10 from Collins et al, 2013] which permits*
12 *comparison of our RCP8.5 results with the CMIP5 multi-model mean.*
13
14 We also add the following caveat to section 4.3.
15 *It is important to note that if the RCP8.5 warming relative to HIST was completely*
16 *offset in the geoBC and geoTiO₂ experiments, the hydrological response would be*
17 *greater than in fig. 6. Using the hydrological sensitivities calculated in section 4.1,*
18 *the precipitation changes relative to HIST would be -0.34 mm/day for geoBC and -*
19 *0.16 mm/day for geoTiO₂.*
20
21 6. Aerosol representation – The reviewer notes that we do not discuss the sensitivity of
22 our results to the choice of size distribution. We have addressed the same issue in our
23 reply to anonymous referee #1, which we repeat below. Specifically, we have
24 compared our results to Ferraro et al (2011), and discussed the likely reasons for the
25 difference in temperature perturbations. The following is added to the Discussions
26 section of this report. *See response 4 to Anonymous Referee #1*
27
28 7. Stratospheric water vapor – The reviewer notes that stratospheric temperature and
29 dynamical changes could perturb the stratospheric water vapor content, with resultant
30 impacts on radiation, chemistry and dynamics. We add the following text to section
31 4.4.
32 *Additionally, an increase in the Tropical Tropopause Layer (TTL) temperature would*
33 *increase the specific humidity of air entering the stratosphere [Dessler et al., 2013].*
34 *Changes to the stratospheric water vapor content could have significant chemical*

1 *and radiative impacts, contributing to ozone depletion via the HO_x cycle and*
2 *stratospheric warming via LW-absorption [Kravitz et al., 2012]. To assess the*
3 *effects of geoengineering on stratospheric water vapor, we calculate the time-*
4 *averaged H₂O mixing ratio averaged between 20°S-20°N and 16-20 km altitude.*
5 *In the HIST era, the H₂O MMR is 4.2 ppmv, in close agreement with HALOE*
6 *observations [Gettelman et al., 2010]. In the 2090s, the average H₂O MMR is 6.3*
7 *ppmv for RCP8.5, 4.8 ppmv for geoSulf, 7.1 ppmv for geoTiO₂, and 32.7 ppmv for*
8 *geoBC. The stratospheric water vapor feedback is therefore greater for geoBC*
9 *and geoTiO₂ than for geoSulf.*

- 10
11 8. Abstract – The reviewer notes that a conclusion that we offer in the abstract is not
12 present in the main text. Specifically, we conclude that the stratospheric heating
13 invoked by BC is so severe as to exclude BC from being a viable candidate particle
14 for SAI. We agree that this is a strong conclusion that should also be in the
15 manuscript. The following has been added to the discussion.

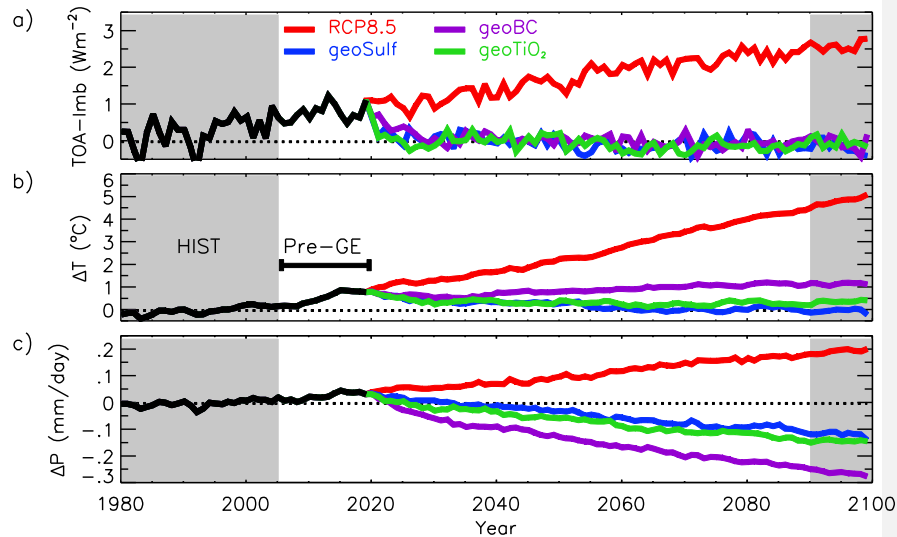
16 *We have shown that, although the distributions of climate changes are similar for the*
17 *3 SAI scenarios, the magnitudes of the changes differ, for instance, BC produces a*
18 *substantially greater stratospheric warming signal with concomitantly greater*
19 *changes to stratospheric dynamics. The severity of the stratospheric temperature*
20 *changes effectively excludes BC from being a viable option for geoengineering.*

- 21
22 9. P44L23 – The reviewer informs us of missing citations. We thank the reviewer for
23 highlighting the missing citations which have been added to the references list (the
24 additional citations are below). Additionally, ‘Collins et al (2014)’ has been changed
25 in the text.

26 *Ramaswamy et al, 2001; Peters et al, 2013; Kravitz et al., 2015; Dhomse et al., 2014;*
27 *Pithan and Mauritsen, 2014; Schmidt et al., 2013; Dessler et al, 2013; Gettelman et*
28 *al., 2010; Niemeier et al., 2013; Liu et al., 2013; Ndour et al., 2008; Koehler et al.,*
29 *2009; Weisenstein et al., 2015; Tang et al., 2014; Davies et al., 2005; Bellouin et al.,*
30 *2007; Priestley et al., 2011; L’Ecuyer et al., 2015; Illingworth et al., 2015; Haywood*
31 *et al., 2011; MacMartin et al., 2013; von Schuckmann et al., 2016*

- 32
33 10. Figure 1 – The reviewer questions why the LW and SW coefficients do not agree in
34 figure 1. This is because the points are plotted at the middle of each spectral

- 1 waveband. Further detail is provided in our reply to the anonymous reader #1
2 (specific response 3). The caption has been altered to include this detail.
3
- 4 11. P50L14 – The reviewer contends with our use of ‘prolong’, as in ‘prolong the
5 stratospheric lifetime’, which was misused here. We replace *prolong* with *maximise*.
6
- 7 12. P50L23 – The reviewer notes that our method for conducting the simulations would
8 benefit from further discussion, which we agree. We did not calculate the injection
9 rate alterations online, this was done in stages. For detail, we simulated 20 model-
10 years at a time and calculated the average TOA_RFI of that period. If the average
11 TOA_RFI exceeded a threshold (0.25 Wm^{-2}), we recalculated the injection rates for
12 that segment of time and restarted the simulation at the start of that time-period. A
13 single ensemble member was used to obtain injection rates for each aerosol; the other
14 2 ensemble members were conducted later. Whether this method is applicable to a
15 real geoengineering scenario is less certain, an ‘online’ algorithm would certainly be a
16 more realistic representation of an actual geoengineering strategy. We go into further
17 detail in specific response 5 to anonymous referee #1, which is then added to the
18 supplement along with a schematic (Section S2 in the Supplement).
19
- 20 13. P53L7 – The reviewer informs us of recent research suggesting that temperature
21 feedbacks contribute to Arctic amplification more than surface-albedo feedbacks. We
22 thank the reviewer for this information and modify the sentence accordingly.
23 *RCP8.5 (Fig. 6a) shows the typical global warming signal of amplified warming at*
24 *high-latitudes due to temperature feedbacks [Pithan and Mauritsen, 2014] and the*
25 *surface-albedo feedback [e.g. Kharin et al., 2013].*
26
- 27 14. P54L7 – The reviewer suggests that we include the global-mean precipitation
28 anomaly time-series in figure 3, which we think is a good idea (the revised figure is
29 plotted below). Additionally the reviewer suggests that we provide normalised values
30 for the precipitation in terms of the temperature anomaly ($\%/^{\circ}\text{C}$). We add this to
31 section 4.1.
32



1

2

In section 4.1 we have added the following paragraph.

3

Fig. 3c shows the global mean precipitation anomaly with respect to the HIST period. The precipitation reduction is greater for BC than for sulfate and titania, despite the positive temperature trend in geoBC (fig. 3b). The hydrological sensitivity to geoengineering, defined as the global mean precipitation change per temperature change, is 2%/°C for sulfate, 2.5%/°C for titania, and 4.6%/°C for BC. The hydrological sensitivity for RCP8.5 is 1.32 %/°C, which is close to the CMIP5 ensemble-mean [Fig. 12.7 from Collins et al, 2013]. For comparison, Bala et al (2008) found a hydrological sensitivity of 2.4%/°C for solar irradiance reduction and 1.4%/°C for CO₂ increase.

12

13

15. P54L9 – The reviewer questions the meaning of the following sentence: “must be ameliorated by additional SW absorption”. We appreciate that this statement is ambiguous and requires elaboration. By this we mean that the SW-absorption for BC exceeds the SW-backscatter for sulfate and titania. The SW radiative perturbation at the tropopause and TOA are therefore greater in geoBC than in geoSulf and geoTiO₂. We have modified the text accordingly.

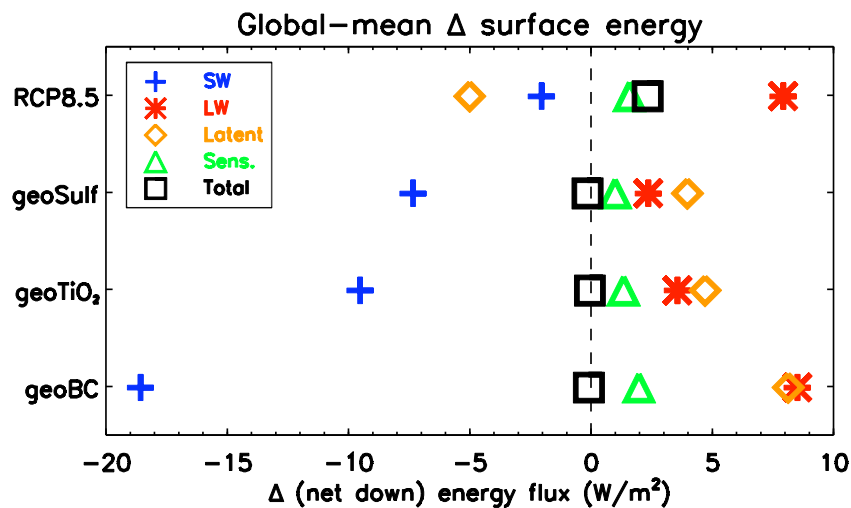
19

In order to maintain TOA-Imb=0, geoBC produces a greater SW perturbation at the tropopause and TOA than geoSulf and geoTiO₂, which is compensated by the increased LW perturbation resulting from stratospheric warming in geoBC. The

21

1 *troposphere is relatively transparent to SW radiation but absorbs efficiently in the LW*
 2 *spectrum, therefore the annual-mean surface radiative forcing in the geoBC*
 3 *experiment is greater (-18.6 W m^{-2}) than for geoSulf or geoTiO₂ (-7.4 and -9.6 W*
 4 *m^{-2} respectively – see Fig. S6 in the Supplement).*

- 5
 6 16. P54L14 – The reviewer is unsure as to how to interpret Fig. S4 in the supplement. We
 7 agree that fig. S4 is perhaps confusing, and have decided to swap it for the following
 8 plot. Please note that when calculating the global-mean surface flux anomalies in the
 9 new plot, we found that the original values given were in error, and have now been
 10 corrected in the text (p 30054). Our analysis is not affected by these changes.



11
 12 **Fig. S6** 2090s global/annual-mean net downward energy flux anomalies at the
 13 *surface (W/m^2). Calculated with respect to piControl*

14 The following additional analysis of Fig. S6 will also be added to the manuscript in
 15 section 4.3.

16 *The reduction in surface SW flux in the RCP8.5 scenario is due to increases in water*
 17 *vapor [Haywood et al., 2011]. Haywood et al (2011) report a clear-sky reduction of*
 18 *-5.7 Wm^{-2} while our study is consistent at a value of -5.4 Wm^{-2} (not plotted). However,*
 19 *in all geoengineering cases, this reduction is comprehensively overwhelmed by*
 20 *aerosol direct effects.*

- 1 17. P55L21 – The reviewer notes that the stratospheric warming under sulfate is the result
2 of net absorption of LW radiation (less emission than absorption). We add the
3 following detail for clarity.
4 *Sulfate predominantly absorbs in the LW and near-infra-red spectrum (Fig. 1a). The*
5 *stratospheric radiative heating in geoSulf is most pronounced in the tropical region,*
6 *where sulfate absorbs outgoing LW radiation from the warm troposphere below, and*
7 *then emits comparatively less radiation from the ambient cold stratosphere [Ferraro*
8 *et al, 2011].*
9
- 10 18. P56L5 – The reviewer questions why we give the maximum sulfate-induced warming
11 as +7°C, when Fig. 10 contravenes this. The maximum sulfate-induced warming is
12 calculated with respect to the RCP8.5 simulation and not to HIST, i.e. displayed in
13 Fig. S6 in the supplement (now Fig. S8). We refer to Figure S6 when giving the
14 maximum BC-induced warming.
15
- 16 19. P56L7 – Tropospheric has been added to tropical circulation
17
- 18 20. P57L11 – The reviewer notes that our analysis of the QBO modification for geoBC
19 would benefit from a rewrite. We agree with this suggestion.
20 *No QBO-like oscillation can be detected in the 10-year time span.*
21
- 22 21. P57L24 – The reviewer notes parallels between our work and Niemeier et al (2013).
23 We thank the reviewer for this notification, and we have added the following to the
24 discussion.
25 *Additionally, producing an equivalent top of the atmosphere radiative perturbation*
26 *with a SW-absorbing aerosol such as BC (or to a lesser extent titania) compared to a*
27 *SW-scatterer such as sulfate, induces a comparatively greater SW forcing at the*
28 *surface. Bala et al (2008) showed that latent heat fluxes compensate for the SW*
29 *reduction at the surface, instigating a deceleration of the hydrological cycle that is*
30 *proportional to the magnitude of the SW reduction. This explains the comparatively*
31 *greater precipitation reduction exhibited by geoBC in figures 6-8. Our results*
32 *complement Niemeier et al (2013), who showed that a LW-absorbing sulfate layer*
33 *would produce a greater hydrological perturbation per TOA SW forcing than a*
34 *simple solar irradiance reduction scenario.*

1
2
3
4
5
6
7
8
9
10
11
12
13
14
15
16

22. P60L10 – The reviewer notes that our conclusion pertaining to the general efficacy of SAI is too definitive. We agree that the statement is a little too strong. We therefore swap “has shown” with “indicates”.

Whilst research indicates that SAI is capable of averting certain climate changes such as surface-warming, SAI provides no amelioration for other climate impacts, such as ocean acidification.

John Dykema

We refer the reader to our specific reply to John Dykema for additional discussion. Below, we highlight the sole change to the manuscript.

1. Precipitation – The reviewerr proposes that we add the model sensitivity into the text for comparison with other GCMs. Thanks for the suggestion, we have added the model sensitivity to the text (section 4.1).

“The precipitation sensitivity for the model is 1.32 %°C, which is close to the CMIP5 ensemble-mean [Fig. 12.7 from Collins et al, 2013].”

1 Climatic Impacts of Stratospheric Geoengineering with 2 Sulfate, Black Carbon and Titania Injection

3

4 **Anthony C. Jones¹, James M. Haywood^{1,2} and Andy Jones²**5 [1]{College of Engineering Maths and Physical Sciences, University of Exeter, Exeter,
6 United Kingdom}

7 [2]{Met Office Hadley Centre, Exeter, United Kingdom}

8 Correspondence to: A. C. Jones (aj247@exeter.ac.uk)

9

10 Abstract

11 In this paper, we examine the potential climatic effects of geoengineering by sulfate, black
12 carbon and titania injection against a baseline RCP8.5 scenario. We use the HadGEM2-CCS
13 model to simulate scenarios in which the top-of-the-atmosphere radiative imbalance due to
14 rising greenhouse gas concentrations is offset by sufficient aerosol injection throughout the
15 2020-2100 period. We find that the global-mean temperature is effectively maintained at
16 historical levels for the entirety of the period for all 3 aerosol-injection scenarios, though
17 there are a wide range of side-effects which are discussed in detail. The most prominent
18 conclusion is that although the BC injection rate necessary to produce an equivalent global
19 mean temperature-response is much lower, the severity of stratospheric temperature changes
20 ($> +70$ °C) and precipitation impacts effectively exclude BC from being a viable option for
21 geoengineering. Additionally, while it has been suggested that titania would be an effective
22 particle because of its high scattering efficiency, it also efficiently absorbs solar ultraviolet
23 radiation producing a significant stratospheric warming ($> +20$ °C). As injection rates and
24 climatic impacts for titania are close to those for sulfate, there appears to be little benefit in
25 terms of climatic influence of using titania when compared to the injection of sulfur dioxide,
26 which has the added benefit of being well modelled through extensive research that has been
27 carried out on naturally occurring explosive volcanic eruptions.

1 **1. Introduction**

2 The climatic impacts of continued greenhouse gas (GHG) emissions are likely to be severe
3 which has prompted countenance of new strategies for tackling GHG-induced global
4 warming [e.g Collins et al., ~~2014~~2013]. Geoengineering strategies, or large-scale climate
5 interventions that aim to reduce global warming, include strategies to sequester atmospheric
6 carbon dioxide – Carbon Dioxide Removal (CDR) methods, and strategies to reduce solar
7 irradiance at Earth’s surface – Solar Radiation Management (SRM) methods [Shepherd et al.,
8 2009]. Stratospheric Aerosol Injection (SAI), an SRM scheme which has received significant
9 attention, involves the enhancement of the stratospheric aerosol layer in order to reflect more
10 sunlight back to space. This scheme mimics large volcanic eruptions such as Mt Pinatubo in
11 1991, which injected approximately 15-20 Tg of sulfur dioxide (SO₂) into the tropical
12 stratosphere and induced a globally averaged surface cooling of around -0.3 °C for the
13 following two years [Stenchikov et al., 2002].

14 Sulfate (SO₄) aerosols have featured predominantly in SAI research because of the volcanic
15 analogue (e.g. in the Geoengineering Model Intercomparison Project, GeoMIP [Kravitz et al.,
16 2013]). General Circulation Model (GCM) simulations suggest that, while sufficient sulfate
17 injection could effectively reduce global-mean temperature, possible side effects include
18 changes to regional precipitation [e.g. Bala et al., 2008; Tilmes et al., 2013], ozone [e.g.
19 Tilmes et al., 2009; Pitari et al., 2014], stratospheric dynamics [Aquila et al., 2014] and sea-
20 ice extent [Berdahl et al., 2014]. Precipitation changes could result from changes to the moist
21 static stability of the atmosphere and a concomitant weakening of the hydrological cycle
22 [Bala et al., 2008], and the regional precipitation changes under GeoMIP simulations have
23 been shown to be reasonably consistent across a range of climate models [Tilmes et al.,
24 2013]. Ozone concentrations could change as a result of enhanced heterogeneous chemistry
25 on the surface of sulfate aerosols or indirectly by changes to the stratospheric dynamics and
26 chemistry [e.g. Tilmes et al., 2009]. Stratospheric dynamical changes could occur as the
27 result of tropical heating in the sulfate layer and by changes to wave propagation from the
28 troposphere [e.g. Aquila et al., 2014].

29 In order to ameliorate the known side-effects of sulfate injection, some authors have proposed
30 alternative aerosols to sulfate [e.g. Teller et al., 1997]. Crutzen (2006) suggested the possible
31 injection of black carbon (BC), which would mimic hypothetical nuclear winter scenarios.
32 One advantage of BC over sulfate is that less mass would be needed for an equivalent
33 radiative forcing [Crutzen, 2006]. BC particles efficiently absorb solar radiation, unlike

1 sulfate which primarily reflects solar radiation [Ferraro et al., 2011]. Alternatively, minerals
2 such as titania (TiO_2), silica (SiO_2) and alumina (Al_2O_3), which have a high refractive index
3 at wavelengths of peak solar radiative flux (~ 550 nm), have also been suggested [Pope et al.,
4 2012]. Although the use of alternative aerosols is not a new suggestion [e.g. Teller et al.,
5 1997], comparatively little research has been conducted on their potential utility. Kravitz et al
6 (2012) simulated a constant BC injection scenario of 1 Tg/yr in the tropics for small radius
7 ($0.03 \mu\text{m}$) and large radius ($0.15 \mu\text{m}$) aerosols. They found that the small particle BC aerosol
8 scenario produced a global surface cooling of -9.45°C , but also induced stratospheric
9 warming $> +60^\circ\text{C}$ and global ozone loss of 50%. The large particle BC aerosol scenario had
10 a negligible climatic impact. Using a fixed dynamical heating (FDH) code, Ferraro et al (2011)
11 compared the stratospheric heating of sulfate, titania, and BC layers for an equivalent
12 instantaneous radiative forcing. Their results showed a tropical stratospheric warming signal
13 for all the aerosols, though much greater in the case of BC. To date, no work has used a
14 comprehensive fully coupled atmosphere-ocean GCM to directly compare the possible
15 climatic impacts of SAI with alternative aerosols to sulfate, which is the motivation for this
16 research.

17 In this work, we simulate the stratospheric injection of sulfate, titania and BC against a
18 baseline RCP8.5 concentrations scenario using a fully-coupled GCM. Titania is selected to
19 represent an efficient light-scattering aerosol and BC is selected as a light-absorbing aerosol.
20 RCP8.5, which is the high-end carbon-intensive CMIP5 scenario, RCP8.5 is selected to
21 give a significant greenhouse effect against which to employ geoengineering, in order to
22 distinguish the climatic impacts specific to each aerosol. Observations have shown that the
23 current global GHG emissions exceed the emissions inherent in RCP8.5 [Peters et al., 2013];
24 therefore our work could be considered as geoengineering against a business-as-usual
25 scenario. Additionally, the next generation of GeoMIP simulations (GeoMIP6) will utilise a
26 carbon-intensive scenario [Kravitz et al., 2015], hence our work will provide a useful
27 supplement to those results. We chose to inject aerosol at a sufficient rate to counterbalance
28 the Top Of the Atmosphere (TOA) global/annual-mean ~~radiative flux~~ Radiative Flux (TOA-
29 RF) imbalance caused by increasing atmospheric GHGs. Our simulation design is similar to
30 the G3 scenario of the Geoengineering Model Intercomparison Project (GeoMIP), which
31 instead used the RCP4.5 concentrations scenario as its baseline and injected sulfate at a
32 sufficient rate to counterbalance GHG radiative forcing [Kravitz et al., 2011]. We analyse the

1 climate changes in the 2090s with respect to a simulated historical period and discuss impacts
2 on a wide range of meteorological parameters.

3

4 **Model**

5 **2.1. The HadGEM2-CCS model**

6 For this investigation, we use the HadGEM2-CCS climate model in a fully coupled
7 atmosphere-ocean mode. HadGEM2-CCS is the high-top configuration of the HadGEM2
8 family of models, and includes a well-resolved stratosphere. The atmosphere component
9 comprises 60 vertical levels extending to 84km and a horizontal resolution of $1.25^\circ \times 1.875^\circ$
10 latitude by longitude respectively. The 40-level ocean component has a horizontal resolution
11 of 1° by 1° from the poles to 30°N/S , with the latitudinal resolution then increasing smoothly
12 to 0.33° at the equator [The HadGEM2 Development Team, 2011]. For this investigation,
13 GHG concentrations, stratospheric ozone, anthropogenic aerosols and aerosol precursor gases
14 are prescribed following the Coupled Model Intercomparison Project phase 5 (CMIP5)
15 [Taylor et al., 2012] protocol, with historical data from 1860-2005 and RCP8.5
16 concentrations from 2005-2100. HadGEM2-CCS contains the aerosol module Coupled
17 Large-scale Aerosol Simulator for Studies in Climate (CLASSIC). The module's sulfur cycle
18 is described in detail in Bellouin et al (2011). Briefly, it includes the oxidation of sulfur
19 dioxide (SO_2) to sulfate aerosol in aqueous and gas phase reactions. Sulfate is represented by
20 Aitken, accumulation and dissolved modes, with hygroscopic growth in the accumulation
21 mode following d'Almeida et al (1991). Aerosol size modes are represented by lognormal
22 size-distributions with a prescribed dry-mode median radius (r_m) and geometric standard
23 deviation (σ).

24

25 **2.2 Stratospheric aerosol microphysical and optical properties**

26 For this investigation, stratospheric sulfate is modelled using the *volc2* size-distribution from
27 Rasch et al (2008) for the sulfate accumulation mode, with $r_m = 0.376 \mu\text{m}$ and $\sigma = 1.25$; the
28 relatively large r_m is chosen to reflect the high concentrations of SO_2 injected in this
29 experiment. ~~Hygroscopic growth is parameterised following Deepak and Gerber (1983).~~

1 CLASSIC includes a tropospheric BC scheme with fresh, aged and in-cloud modes [Bellouin
2 et al, 2011]. We introduce an additional non-hygroscopic stratospheric BC component and
3 prescribe a lognormal size-distribution with $r_m = 0.0118 \mu\text{m}$ and $\sigma = 2.0$, which is taken from
4 tropospheric BC observations [Deepak and Gerber, 1983]. We prescribe a density for BC of
5 1000 kg/m^3 and take refractive indices from a World Meteorological Organisation report
6 [Deepak and Gerber, 1983].

7 For stratospheric titania, we assume the non-hygroscopic lognormal size distribution of Pope
8 et al. (2012) with $r_m = 0.045 \mu\text{m}$ and $\sigma = 1.8$. This size-distribution was selected to give the
9 titania aerosol a high scattering efficiency, as shown by Pope et al (2012). We prescribe a
10 density for titania of 4230 kg/m^3 [Pope et al, 2012], and for the refractive indices we follow
11 Ferraro et al (2011) and use the average of the extra-ordinary and ordinary values from
12 Ribarsky (1984, 1985).

13 The specific absorption (k_{abs}) and scattering (k_{sca}) coefficients for sulfate (accumulation/dry-
14 mode), titania and BC are plotted in Fig. 1 as a function of wavelength. For sulfate, the
15 specific extinction coefficient (k_{ext}) at 500nm of $3200 \text{ m}^2/\text{kg kg/m}^3$ -and single scattering
16 albedo (ω_0) of 1 reflects the non-absorbing properties of sulfate. Although titania's 500nm
17 scattering efficiency ($k_{\text{sca}} = 3850 \text{ m}^2/\text{kg kg/m}^3$) is greater than sulfate's in this instance, titania
18 additionally absorbs SW radiation ($k_{\text{abs}} = 2000 \text{ m}^2/\text{kg kg/m}^3$ at 250 nm, and $k_{\text{abs}} = 600$
19 $\text{m}^2/\text{kg kg/m}^3$ at 500 nm) which can be explained by the band-theory of solids [Yang et al,
20 2003]. Thus titania is partially absorbing. Our modelled BC efficiently absorbs SW radiation
21 ($k_{\text{abs}} = 8300 \text{ m}^2/\text{kg kg/m}^3$ at 500nm) but also produces a non-negligible SW scattering effect
22 ($k_{\text{sca}} = 2500 \text{ m}^2/\text{kg kg/m}^3$ at 500nm) which is comparable in magnitude to the equivalent
23 scattering efficiency of both titania and sulfate. Therefore, to describe titania as an efficient
24 light-scatterer and/or BC as an efficient light-absorber is an over-simplification.

25 Our choice of particle size and density will impact the aerosol's gravitational sedimentation
26 rate and therefore its atmospheric residence time (the sedimentation rate is also a property of
27 the local atmospheric conditions) [Rasch et al., 2008]. To determine the importance of our
28 choice of aerosol properties, we have calculated the respective gravitational sedimentation
29 rates by using the method of Pruppacher and Klett (1979) (which utilises Stoke's law) and
30 incorporating temperature and pressure values from the International Standard Atmosphere
31 [ICAO, 1993] (Supplementary-Fig. S1 in the Supplement). We find that the average
32 sedimentation rates between 18-26 km altitude for our prescribed sulfate, titania, and BC are

1 23, 9.5 and 0.75 m/day respectively, and the equivalent rates between 26-30 km are 52, 22,
2 and 1.8 m/day. Therefore, one would expect BC to be advected to much higher altitudes than
3 sulfate in these simulations. For perspective, Schoeberl et al (2008) deduced from
4 observations that the atmospheric tropical vertical velocity between 18-26 km has an upper
5 limit of 35 m/day, and the equivalent velocity between 26-30 km is below 61 m/day.

6

7 **Method**

8 We first validated the model's stratospheric sulfate scheme by simulating the Mt Pinatubo
9 eruption and then comparing the results with observations. These simulations comprised a
10 10-member ensemble in which 20 Tg[SO₂] is injected between 16-18 km over a single day in
11 June 1991, following the method of Aquila et al (2012). Figure 2a shows the global/annual-
12 mean sulfate aerosol optical depth (AOD) anomaly for the HadGEM2-ensemble and for
13 AVHRR and SAGE-II observations. The model clearly captures the peak AOD from the
14 AVHRR data, and the exponential decline thereafter. Figures 2b-d show the zonal-mean
15 AOD anomaly for the same time period. The agreement between the model and observed
16 AOD is reasonable. Some differences in the temporal evolution of the AODs in the model
17 and the observations are due to the almost concurrent eruption of Cerro Hudson which
18 injected approximately 3.3Tg[SO₂] into the southern hemisphere [Deshler and Anderson-
19 Sprecher, 2006]. This relatively close agreement between observations and HadGEM2
20 estimates, together with other modelling studies of other volcanic eruptions [Haywood et al.,
21 2010] suggests that the model is a useful tool for stratospheric geoengineering simulations.

22 The geoengineering investigation was based on a 240-year Pre-Industrial Control simulation
23 (forced by constant 1860's GHGs and aerosol emissions) and historical simulations for the
24 period 1860-2005 following CMIP5 [Taylor et al., 2012] protocol followed by RCP8.5
25 emission specified from 2005-2019. Leading on from these simulations, we performed 3-
26 member ensembles for the period 2020-2100 for: RCP8.5 only, RCP8.5 with SO₂ injection
27 (~~G3S-geoSulf~~), RCP8.5 with TiO₂ injection (~~geoTiO₂-G3TiO₂~~), and RCP8.5 with BC injection
28 (~~G3BC-geoBC~~). ~~The G3 nomenclature is adopted because of the similarity of our simulations~~
29 ~~to the G3 experiments of GeoMIP although the original G3 experiments were compared~~
30 ~~against RCP4.5 and the geoengineering period was terminated at 2070 [Kravitz et al., 2011].~~
31 Aerosol (or gaseous SO₂ for the ~~G3S-geoSulf~~ scenario) was injected at a constant rate
32 between 23-28 km altitude in a single vertical column at the equator. The injection altitude

1 and location were chosen to ~~prolong~~ maximise the stratospheric lifetime of the aerosol, which
2 is transported poleward by the upper branch of the Brewer-Dobson circulation [Niemeier et
3 al., 2011], and therefore make the geoengineering approach reasonably efficient.

4 We inject aerosol at such a rate as to maintain the top-of-the-atmosphere (TOA) net
5 radiation at piControl levels. Specifically, we define the TOA radiative flux Imbalance
6 (TOA-Imb) as the annual/global-mean TOA net radiation (incoming SW minus outgoing
7 LW+SW) minus the average TOA net radiation of the piControl period. By sufficient
8 aerosol injection, we aim to maintain TOA-Imb=0. This scenario represents our
9 interpretation of ‘equal amount of geoengineering’ for each aerosol. The advantage of
10 returning net radiation to piControl levels (rather than completely equilibrating TOA
11 fluxes) is that piControl had already been simulated comprehensively for CMIP5 (240
12 model-years), hence permitting robust statistics to be calculated. The TOA radiative
13 imbalance is a metric that satellites are able to measure (e.g. CERES [L’Ecuyer et al.,
14 2015] and EarthCare [Illingworth et al, 2015]), albeit with +/- 3 W/m² accuracy at
15 present [Priestley et al, 2011; von Schuckmann et al., 2016]. Therefore our target could
16 be applicable to an actual SAI scenario. In contrast, Radiative Forcing (RF) (the net
17 radiation perturbation at the tropopause from some external forcing, after stratospheric
18 adjustment), cannot be directly measured by satellites and therefore it would be difficult
19 to obtain a specified radiative forcing in an actual SAI scenario. Of course, other metrics
20 could be chosen [e.g. MacMartin et al., 2013], with each metric having its own
21 signal/noise characteristic.

22 To determine the injection rates required to maintain TOA-~~Imb~~~~RF~~ balance, we first
23 conducted ~~40~~15-year atmosphere-only simulations of 1 Tg aerosol (or SO₂ for sulfate)
24 injection per year to calculate the specific radiative effect for each aerosol. We then used the
25 radiative effect to calculate the injection rate necessary to offset the RCP8.5 anthropogenic
26 radiative forcing (ARF) for the 2020-2100 period (with ARF values from Meinshausen et al
27 (2011)). We used the ARF to estimate the injection rates required to produce TOA-Imb=0 as
28 this produces reasonable initial injection rates. As the geoengineering simulations progressed,
29 we altered the injection rate when necessary to ensure that TOA-~~RF~~~~Imb~~ balance was
30 maintained- (Fig. S2 in the Supplement). A detailed description of our methods is provided in
31 the supplementary material (Section S2).

Formatted: Line spacing: 1.5 lines

Our analysis focuses initially on the temporal evolution of the TOA-~~RF-Imb~~ and global mean temperature changes to show that our simulations provide plausible counterbalances to global mean temperature changes under RCP8.5. However, our main focus is on the differences between ~~the a~~ recent historical period (1980-2005) (hereafter denoted HIST) and the geoengineering experiments during the period 2090-2100, with an emphasis on different geographical patterns. ~~As we were not explicitly attempting to reach a specific global mean temperature, the choice of reference period was left until after the geoengineering simulations had been completed. We then selected a recent historical period from which the 2090s global-mean temperature anomaly for geoSulf was negligible (Fig. 3b). The HIST period selected is close to the historical control period used in the IPCC AR5 report (1986-2005) [e.g. Fig. 12.10 from Collins et al., 2013] which facilitates comparison of our RCP8.5 climate changes with the CMIP5 multi-model means.~~

Results

4.1 Effectiveness at maintaining global mean TOA-~~RF-Imb~~ and near surface temperature

Figure 3 shows the global/annual-mean TOA-~~RF-Imb imbalance~~ and near-surface air temperature anomaly for the geoengineering and RCP8.5 simulations, with respect to the HIST period. For all of the geoengineering simulations we were able to maintain TOA-~~Imb \approx 0 RF-balance~~ for the entirety of the 80-year period (Fig. 3a). For ~~geoSulf, geoTiO₂, G3S, G3TiO₂ and G3BCgeoBC~~, the TOA-~~RF-Imb~~ was maintained within +/-0.21, +/-0.18 and +/-0.20 Wm⁻², respectively (1 standard deviation throughout the 2020-2100 period).

~~However, the near-surface global temperature response differs between the aerosols with a greater cooling effect for sulfate than for titania or BC. This is due to the absorption of radiation by BC (and a lesser extent the absorption by titania) heating the stratosphere which then increases the terrestrial longwave radiation entering the troposphere reducing the tropopause RF. As noted in several Intergovernmental Panel on Climate Change reports [e.g. Ramaswamy et al., 2001; Forster et al., 2007], it is the global mean tropopause RF rather than the TOA RF that is proportional to global mean surface temperature changes. Further analysis of stratospheric temperature changes will be provided in section 4.4.~~

~~The near-surface global temperature response differs between the aerosols with a greater cooling trend for sulfate than for titania or BC (Fig. 3b). To determine the cause of the~~

Formatted: Line spacing: 1.5 lines

1 anomalous warming in geoBC, we assess the net radiation at the top of the atmosphere
2 for 2020-2100. Fig. S3 in the Supplement shows the global-mean net-downward
3 radiation anomaly for the geoengineering experiments, evaluated at the TOA and the
4 tropopause; and the global-mean net-downward heat flux anomaly at the surface. The
5 radiation changes at the TOA and tropopause, and the heat flux anomaly at the surface,
6 are comparable for the geoSulf and geoTiO₂ experiments for the duration of 2020-2100.
7 In contrast, geoBC exhibits an increasingly positive net radiation anomaly at the
8 tropopause (+0.2 W/m² averaged over 2020-2100) despite the negligible TOA radiation
9 anomaly. After stratospheric temperature adjustment, radiative perturbations at the TOA
10 and tropopause are equal for a given climate forcing, which implies that the consistently
11 non-adjusted stratosphere (due primarily to increasing aerosol injection rates) is
12 responsible for the differences in TOA and tropopause radiative perturbations in geoBC.
13 This implies that if we had injected aerosol sufficiently to produce an equal radiative
14 effect at the tropopause, the temperature trends for the geoengineering experiments in
15 Fig. 3 would have been more comparable. If we were to choose stabilisation of temperature
16 as our basic metric, then one could approximate the results by simply scaling the results by
17 the ratio of the temperature perturbation relative to 1980-2005 to that for geoSulf. The scaling
18 would be 1 (by design) for geoSulf, 1.1 for geoTiO₂ and 1.28 for geoBC. If the metric chosen
19 were instead to keep the global mean precipitation the same, then the scaling would be 1 (by
20 design) for geoSulf, 0.91 geoTiO₂ and 0.68 for geoBC. However, we shall see that the
21 changes in many of the variables we consider are dominated by large scale changes in the
22 spatial patterns of response rather than the 10-30% changes in magnitude of the response that
23 applying such a scaling would induce. We therefore choose to present un-scaled results here
24 but caveat that such a scaling could be applied should we wish to apply a different metric.
25 From Fig. 3b, geoSulf exhibits a near-surface air cooling trend with respect to 2020 despite a
26 net gain of atmospheric energy, which is likely due to an uneven vertical distribution of this
27 energy gain.

28 Fig. 3c shows the global mean precipitation anomaly with respect to the HIST period.
29 The precipitation reduction is greater for BC than for sulfate and titania, despite the
30 positive temperature trend in geoBC (Fig. 3b). The hydrological sensitivity to
31 geoengineering, defined as the global mean precipitation change per unit temperature
32 change, is 2%/°C for sulfate, 2.5%/°C for titania, and 4.6%/°C for BC. The hydrological
33 sensitivity for RCP8.5 is 1.32 %/°C, which is close to the CMIP5 ensemble-mean [Fig. 12.7

1 [from Collins et al., 2013\]. For comparison, Bala et al \(2008\) found a hydrological](#)
2 [sensitivity of 2.4%/°C for solar irradiance reduction and 1.4%/°C for CO₂ increase.](#)

4 **4.2 Aerosol distribution**

5 The time-averaged injection rates for the 2090s period are 14 Tg[SO₂]/yr, 5.8 Tg/yr and 0.81
6 Tg/yr for [geoSulf](#), [geoTiO₂](#), [G3S](#), [G3TiO₂](#) and [G3BCgeoBC](#), respectively. This SO₂ injection
7 rate is approximately equivalent to 1 Mt Pinatubo eruption per year [Dhomse et al, 2014].

8 These injection rates equate to global aerosol mass-burden anomalies of 49.5, 20.2, and 5.1
9 Tg for [geoSulf](#), [geoTiO₂](#), [G3S](#), [G3TiO₂](#) and [G3BCgeoBC](#), respectively. The [G3BC-geoBC](#)
10 mass burden is comparable to the equilibrium burdens of the high-altitude (HA) and small-
11 radius (SmR) experiments from Kravitz et al (2012), although they injected BC at a constant
12 rate of 1 Tg/yr, around 20% higher than in our study. Figure 4 shows the 2090s annual, June-
13 July-August (JJA) and December-January-February (DJF) aerosol mass concentration
14 anomalies (annual mean aerosol optical depths are shown in [Supplementary-Fig. S4 in the](#)
15 [Supplement-2](#)). Peak sulfate concentrations are found at the injection region at the equator
16 (Figs. 4a,d,g) and over the winter pole. Titania and BC reach greater altitudes than sulfate
17 (>50 km), which is due to their smaller size-distributions and self-lofting from SW-
18 absorption [Kravitz et al, 2012]. While sulfate aerosol concentrations are highest at the
19 equator, the highest concentrations of BC are found in the polar stratosphere. This is because
20 the larger particle size of the sulfate aerosol is subject to a larger sedimentation velocity ([see](#)
21 [Supplementary-Fig. S1 in the Supplement-4](#)) and thus a greater fraction of aerosol is removed
22 close to the source region. The results from titania suggest a spatial distribution intermediate
23 between sulfate and BC owing to the intermediate size distribution.

24 Figure 5 shows the total annual, JJA and DJF aerosol deposition anomalies averaged over the
25 2090s (the seasonal cycle of the deposition anomalies are shown in [Supplementary-Fig. S5 in](#)
26 [the Supplement-3](#)). Sulfate is predominantly deposited in the Northern Hemisphere (NH)
27 extratropics in the boreal spring and summer (Fig. 5d) which is likely attributable to
28 tropopause fold events in the lower branch of the Brewer-Dobson circulation (BDC) [Kravitz
29 et al., 2012]. In contrast, Titania and BC are primarily deposited at high latitudes in the polar
30 winter, which is attributable to the diabatic descent of air in the deep branch of the BDC [e.g.
31 Tegtmeier et al., 2008]. Kravitz et al (2012) also found in their SmR experiment that BC
32 deposition was limited to the polar regions, but their maximum deposition was during polar

1 summer rather than polar winter. The global/annual-mean deposition rates of sulfate and BC
 2 from geoengineering are 37 and 1.5 mg/m²/yr, respectively. These amounts may be compared
 3 with 231 and 12.7 mg/m²/yr from non-geoengineering sources, amounting to increases of 16
 4 % and 12 % respectively. The global/annual-mean deposition rate for titania is 11 mg/m²/yr.

6 **4.3 Temperature and precipitation**

7 Figure 6 shows the annual mean near-surface air temperature (Figs. 6a-d) and precipitation
 8 anomalies (Figs. 6e-h) with respect to HIST. RCP8.5 (Fig. 6a) shows the typical global
 9 warming signal of amplified warming at high-latitudes due to temperature feedbacks
 10 [Pithan and Mauritsen, 2014] and the positive snowsurface-albedo feedback [e.g. Kharin et
 11 al., 2013]. This results in an annual mean warming of +11.3 °C averaged over the Arctic
 12 region (> 60 °N) and an average NH land warming of +7.3 °C. This figure provides an
 13 alarming picture of the change in global mean temperature by the end of this century should
 14 global society follow the RCP8.5 (essentially a business as usual) pathway. All 3 SAI
 15 experiments produce a surface-cooling with respect to RCP8.5, with G3S-geoSulf exhibiting
 16 the greatest global-mean cooling effect of -4.85 °C, considering TOA-Imb is balanced for
 17 each geoengineering experiment. The latitudinal distribution of cooling varies markedly
 18 between the SAI experiments, with relative tropical cooling for G3S-geoSulf and
 19 geoTiO₂-G3TiO₂ (Figs. 6b,d) and polar cooling for G3BC-geoBC (Fig. 6c). Defining the ‘SAI
 20 cooling effect’ as the temperature difference between SAI and RCP8.5, the ratio of cooling
 21 effect at high latitudes (> 60°) between G3BC-geoBC and G3S-geoSulf is 1.19 and between
 22 G3BC-geoBC and G3TiO₂-geoTiO₂ is 1.23. In the tropics and mid-latitudes (< 60°) the
 23 equivalent ratios are 0.64 and 0.71 respectively. The high-latitude cooling in the case of
 24 G3BC-geoBC is attributable to the zonal distribution of BC (Figs. 4c,f,i) which is more
 25 evenly spread over the stratosphere than for G3S-geoSulf and G3TiO₂-geoTiO₂. The result is a
 26 greater surface SW forcing at high-latitudes in the summer hemisphere for G3BC-geoBC. For
 27 instance, in the Arctic (>60°N) in JJA, the surface SW forcing is -25.65 Wm⁻² in G3BC
 28 geoBC and -3.3 and -6.55 Wm⁻² in G3S-geoSulf and G3TiO₂-geoTiO₂ respectively.

29 Although the global-mean precipitation rate increases for the RCP8.5 scenario (Fig. 6e),
 30 certain regions such as the Amazon basin exhibit a drying trend. This is in line with the
 31 CMIP5 multi-model projections documented in the Intergovernmental Panel on Climate
 32 Change 5th assessment report (IPCC AR5) [e.g. Fig. 12.710 from Collins et al., 2013]. All of

1 the SAI experiments show a global-mean precipitation reduction with respect to both HIST
 2 and RCP8.5 (Figs. 6f-h), which is due to the deceleration of the hydrological cycle and is a
 3 robust model response to SAI [e.g. Yu et al., 2015; Tilmes et al., 2013; Bala et al., 2008]. The
 4 magnitude of the precipitation changes are greater for ~~G3BC-geoBC~~ than for ~~G3S-geoSulf~~ or
 5 ~~G3TiO₂geoTiO₂~~; for instance, the global mean precipitation anomaly is -0.26 mm/day for
 6 ~~G3BC-geoBC~~ compared to -0.12 mm/day for ~~G3S-geoSulf~~ and -0.14 mm/day for
 7 ~~G3TiO₂geoTiO₂~~. ~~This is because the stratospheric heating in G3BC applies an additional LW~~
 8 ~~forcing at the tropopause and TOA which must be ameliorated by additional SW absorption~~
 9 ~~in order to maintain radiative balance [Ferraro et al., 2011]. In order to maintain TOA-~~
 10 ~~Imb=0, BC must produce a greater SW perturbation at the tropopause and at the TOA~~
 11 ~~than sulfate or titania, which is compensated by the increased LW perturbation resulting~~
 12 ~~from stratospheric warming.~~ The troposphere is relatively transparent to SW radiation but
 13 absorbs efficiently in the LW spectrum, therefore the annual-mean surface radiative forcing
 14 in the ~~G3BC-geoBC~~ experiment is greater (~~-18.6 -10.2~~ Wm⁻²) than for ~~G3S-geoSulf~~ or
 15 ~~geoTiO₂G3TiO₂~~ (~~-5.1 -7.4~~ and ~~-6.06 -9.6~~ Wm⁻² respectively - see ~~Supplementary-Fig. S6 in~~
 16 ~~the Supplement-4~~). Bala et al (2008) showed that the magnitude of the precipitation response
 17 is dependent on the surface radiative imbalance; therefore the precipitation reduction is
 18 amplified in ~~G3BC-geoBC~~. ~~It is important to note that if the RCP8.5 warming relative to~~
 19 ~~HIST was completely offset in the geoBC and geoTiO₂ experiments, the hydrological~~
 20 ~~response would be greater than in Fig. 6. Using the hydrological sensitivities calculated in~~
 21 ~~section 4.1, the precipitation changes relative to HIST would be -0.34 mm/day for geoBC and~~
 22 ~~-0.16 mm/day for geoTiO₂. From Fig. S6 in the Supplement, the reduction in surface SW~~
 23 ~~flux in the RCP8.5 scenario is due to increases in water vapor [Haywood et al., 2011].~~
 24 ~~Haywood et al (2011) report a clear-sky reduction of -5.7 W/m² while our study is~~
 25 ~~consistent at a value of -5.4 W/m² (not plotted). However, in all geoengineering cases,~~
 26 ~~this reduction is comprehensively overwhelmed by aerosol direct effects.~~

27 Figure 7 shows the JJA temperature (Figs. 7a-d) and precipitation (Figs. 7e-h) anomalies. In
 28 the ~~G3S-geoSulf~~ and ~~geoTiO₂G3TiO₂~~ scenarios, the temperature is effectively maintained at
 29 HIST levels (Figs. 7b,d). However, a slight bias towards high-latitude NH warming in ~~G3S~~
 30 ~~geoSulf~~ and ~~geoTiO₂G3TiO₂~~ results in a northward displacement of the Inter-Tropical
 31 Convergence Zone (ITCZ), which is exemplified by the Sahelian precipitation increase in
 32 Figs. 7f,h. This phenomenon was noted by Haywood et al (2013) and has been observed after
 33 large hemispherically asymmetric volcanic eruptions [~~Oman et al., 2006~~]. Although the

1 | general pattern of precipitation change is similar for the 3 SAI scenarios, G3BC-geoBC again
2 | displays a greater drying signal, with 80% of the total land area experiencing a JJA
3 | precipitation reduction in G3BC-geoBC compared to 70% for geoTiO₂G3TiO₂, 57% for G3S
4 | geoSulf and 52% for RCP8.5.

5 | Figure 8 shows the DJF temperature (Figs. 8a-d) and precipitation (Figs. 8e-h) anomalies.

6 | The temperature reduction over Greenland in G3BC-geoBC (Fig. 8c) is due to the significant
7 | decrease in downwelling SW radiation at the surface during the Arctic sea-ice formation
8 | season (September-October-November), which leads to a positive sea-ice albedo feedback
9 | and further localised cooling. This inference is corroborated by Fig. 9, which shows the
10 | Arctic DJF sea-ice extent in terms of the average DJF sea-ice boundary (the Antarctic DJF
11 | sea-ice extent is shown in Supplementary-Fig. S7 in the Supplement-5). The sea-ice boundary
12 | in G3BC-geoBC (Fig. 9c) extends to well below Greenland, and the total sea-ice extent
13 | anomaly is +1.72 million km² which vastly exceeds the HIST standard deviation of +/- 0.52
14 | million km². In comparison, the sea-ice extent anomaly of -11 million km² for RCP8.5 (Fig.
15 | 9a) marks a reduction by 43% of the total HIST sea-ice extent. Returning to Fig. 8, the
16 | poleward shift in the NH extratropical rain-belt over the Atlantic in RCP8.5 (Fig. 8e) is a
17 | robust result of GHG-induced global warming and is related to storm track displacement
18 | [Lombardo et al, 2015]. This same response is evident in the geoengineering simulations
19 | (Figs. 8f-h), although to a much lesser extent in G3S-geoSulf and geoTiO₂G3TiO₂.

21 | **4.4 Stratospheric changes**

22 | Figure 10 shows the zonal-mean temperature change as a function of latitude and altitude for
23 | the JJA and DJF seasons. The stratospheric cooling in conjunction with tropospheric
24 | warming in RCP8.5 (Figs. 10a,e) is a robust result of increasing GHG-concentrations [e.g.
25 | Schmidt et al., 2013]. Aerosols directly affect temperature by absorbing radiation, and
26 | indirectly by scattering radiation and by ambient dynamical and chemical changes [Carslaw
27 | and Kärcher., 2006].- Sulfate predominantly absorbs in the LW and near-infrared spectrum
28 | (Fig. 1a), ~~therefore the stratospheric radiative heating in G3S is mostly confined to the~~
29 | ~~tropical region, where the stratosphere is significantly colder than the underlying warm~~
30 | ~~troposphere [Ferraro et al, 2011].- The stratospheric radiative heating in geoSulf is most~~
31 | pronounced in the tropical region, where sulfate absorbs outgoing LW radiation from the
32 | warm troposphere below, and then emits comparatively less radiation from the ambient

1 | [cold stratosphere \[Ferraro et al., 2011\]](#). In contrast, titania and BC absorb in both the SW
2 | and LW spectrum (Figs. 1b,c), and therefore preferentially warm the summer-hemisphere and
3 | tropical stratosphere, where solar radiation is most prevalent. ~~G3BC~~-[geoBC](#) produces the
4 | most significant warming effect, with an average stratospheric (15-50 km altitude)
5 | temperature increase of +33 °C and a maximum temperature increase of +68 °C, which
6 | occurs in JJA (Figs. 10c,g). The maximum BC-induced heating relative to the baseline
7 | RCP8.5 scenario is +76 °C (~~Supplementary-Fig. S8 in the Supplement~~6), which is
8 | comparable to the ~80 °C temperature change Kravitz et al (2012) found in their SmR
9 | scenario. For comparison, the maximum sulfate-induced and titania-induced heating relative
10 | to RCP8.5 are far more modest at +7 °C and +22 °C, respectively.

11 | A warming of the lower tropical stratosphere could have multiple climatic repercussions such
12 | as a weakening of the [tropospheric](#) tropical circulation [Ferraro et al., 2014], strengthening of
13 | the polar vortex [Driscoll et al., 2012] and modification of the Quasi-Biennial Oscillation
14 | (QBO) [Aquila et al., 2014]. [Additionally, an increase in the Tropical Tropopause Layer](#)
15 | [\(TTL\) temperature would increase the specific humidity of air entering the stratosphere](#)
16 | [\[Dessler et al., 2013\]. Changes to the stratospheric water vapor content could have](#)
17 | [significant chemical and radiative impacts, contributing to ozone depletion via the HO_x](#)
18 | [cycle and stratospheric warming via LW-absorption \[Kravitz et al., 2012\]. To assess the](#)
19 | [effects of geoeengineering on stratospheric water vapor, we calculate the time-averaged](#)
20 | [H₂O mixing ratio averaged between 20°S-20°N and 16-20 km altitude. In the HIST era,](#)
21 | [the H₂O MMR is 4.2 ppmv, in close agreement with HALOE observations \[Gettelman et](#)
22 | [al., 2010\]. In the 2090s, the average H₂O MMR is 6.3 ppmv for RCP8.5, 4.8 ppmv for](#)
23 | [geoSulf, 7.1 ppmv for geoTiO₂, and 32.7 ppmv for geoBC. The stratospheric water vapor](#)
24 | [feedback is therefore greater for geoBC and geoTiO₂ than for geoSulf.](#)

25 | A strengthening of the polar vortex could be instigated by an increased temperature gradient
26 | between the tropical/mid-latitude and polar stratospheres, a phenomenon which was observed
27 | after the Pinatubo eruption [Stenchikov et al., 2002]. We concentrate on the Arctic wintertime
28 | (DJF) response to SAI, and adopt a similar metric to that used by Ferraro et al (2011) to
29 | determine the stratospheric temperature gradient. Explicitly, we determine the difference in
30 | temperature between 20°N-20°S (Tropics) and 50°N-90°N (North Pole) at 17-22 km altitude
31 | in the DJF season. Using this metric, the change in temperature gradients for ~~G3BC~~-[geoBC](#),
32 | ~~G3S~~-[geoSulf](#) and ~~G3TiO₂~~-[geoTiO₂](#) are +10.4 °C, +7 °C, and +10.1 °C, respectively, indicating
33 | a steeper temperature gradient between the tropics and poles. Additionally, Fig. 11 shows the

1 50hPa DJF geopotential height anomalies over the Arctic for RCP8.5 and the 3 SAI
2 experiments. The negative geopotential height anomaly centered over the North Pole in all
3 the SAI experiments is indicative of a strengthened polar night jet and a positive Arctic
4 Oscillation phase [Stenchikov et al, 2002]. The DJF zonal-mean zonal-wind anomaly
5 ([Supplementary-Fig. S9 in the Supplement-7](#)) substantiates our inference of a strengthened
6 polar-night jet under SAI, with increased zonal windspeeds at 65°N / 40km altitude of 62 m/s,
7 17 m/s, and 37 m/s for [geoBC](#), [geoSulf](#)~~G3BC~~, ~~G3S~~, and [geoTiO₂](#)~~G3TiO₂~~ respectively.

8 The Quasi-Biennial Oscillation (QBO) is a periodic change in the equatorial zonal wind
9 pattern in the stratosphere, which fluctuates between easterly and westerly-shear phases
10 [Baldwin et al., 2001]. Aquila et al (2014) showed that radiative heating in the aerosol layer
11 could prolong the westerly-phase of the QBO (where the phase is defined at 40 hPa) by
12 enhancing the residual-mean upwelling motion and strengthening the westerly winds.
13 HadGEM2-CCS includes a non-orographic gravity wave scheme that permits the model to
14 internally generate a QBO and is therefore capable of assessing QBO changes [The
15 HadGEM2 Development Team, 2011]. The average QBO period for the HIST-era ensemble
16 is 27 months ([Supplementary-Fig. S10 in the Supplement8](#)) which agrees closely with
17 observations [e.g. Baldwin et al., 2001]. Figure 12 shows the 2090s QBO timeseries for one
18 ensemble member of the RCP8.5 and SAI experiments ([Supplementary-Figs. S11a,9a,b in the](#)
19 [Supplement](#) -show the QBO timeseries for the other 2 ensemble members). The average QBO
20 periods for this timespan, which are determined using all 3-ensemble members, are 20
21 months for RCP8.5, 31 months for [G3S-geoSulf](#) and 36 months for [geoTiO₂](#)~~G3TiO₂~~. For
22 [G3BC-geoBC](#), the [no QBO-like oscillation can be detected in the 10-year time](#)
23 [span, periodicity of the QBO extends beyond the 10-year span considered here](#), suggesting a
24 persistent westerly-phase such as observed by Aquila et al (2014) in their G₅^{22-25km} scenario.
25 In their HadGEM2-CC simulations, Kawatani and Hamilton (2013) also observed a decline
26 in the QBO period for the RCP8.5 scenario, although they were unable to provide a reason
27 for this. A robust inference from this work is that the magnitude of SAI's impact on
28 stratospheric zonal winds correlates with the magnitude of the stratospheric warming.

30 Discussion

31 In this work, we have assessed the climatic impacts of sulfate, black carbon and titania-
32 injection against a baseline RCP8.5 scenario, by comparing the 2090s climate with a

1 simulated historical period. We have shown that, although the distribution of climate changes
2 are similar for the 3 SAI scenarios, the magnitude of the changes differ, for instance BC
3 produces a substantially greater stratospheric warming signal with concomitantly greater
4 changes to stratospheric dynamics. The severity of the stratospheric temperature changes
5 effectively excludes BC from being a viable option for geoengineering. Additionally, we
6 have shown that ~~Additionally,~~ producing an equivalent top of the atmosphere radiative
7 perturbation with a SW-absorbing aerosol such as BC (or to a lesser extent titania) compared
8 to a SW-scattering aerosol ~~scatterer~~ such as sulfate, induces a comparatively ~~produces a~~
9 greater SW forcing at the surface. Bala et al (2008) showed that reduced latent heat fluxes
10 compensate for the SW reduction at the surface, instigating a deceleration of the hydrological
11 cycle that is proportional to the magnitude of the SW reduction. This explains the
12 comparatively greater precipitation reduction exhibited by geoBC in figures 6-8. Our results
13 complement Niemeier et al (2013), who showed that a LW-absorbing sulfate layer would
14 produce a greater hydrological perturbation per TOA SW forcing than a simple solar
15 irradiance reduction scenario, which could further disrupt the hydrological cycle beyond the
16 hydrological perturbation expected for sulfate injection. The ~~G3BC-geoBC~~ scenario displays
17 a greater cooling at high-latitudes than the ~~G3S-geoSulf~~ and ~~geoTiO₂G3TiO₂~~ scenarios (Figs.
18 6-8), which comparatively exhibit a net tropical cooling. This raises the question of whether a
19 combination of aerosols could potentially be injected to produce a zonally-homogeneous
20 cooling if necessary. Although SAI with sulfate and titania effectively maintains the regional
21 distribution of temperature at HIST levels, with a slight residual warming at high latitudes,
22 the hydrological cycle decelerates substantially in all SAI scenarios which is exemplified by a
23 global-mean reduction in precipitation. However, annual-minimum sea-ice extent in both
24 hemispheres and global-mean thermosteric sea-level (~~Supplementary Fig. S12 in the~~
25 Supplement) ~~are 40) is~~ almost entirely maintained at HIST levels for all SAI scenarios.
26 We find that sulfate induces less stratospheric warming than titania. In contrast, Ferraro et al
27 (2011) found that the peak stratospheric warming for titania was approximately a third of that
28 from sulfate. Although the different climatologies, model configurations, and aerosol spatial
29 distributions will contribute to the difference in stratospheric temperature adjustment between
30 our and Ferraro's work, the primary reason for the disparity is likely to be the aerosol size
31 distributions. Our titania is smaller (median radius = 0.045 μm compared to 0.1 μm for
32 Ferraro et al (2011)) and therefore scatters and absorbs SW more efficiently, producing a
33 greater localised 'solar' warming. Their sulfate distribution contains a larger spread ($\sigma = 2.0$

1 for Ferraro et al (2011) compared to $\sigma = 1.25$ here), resulting in more coarse-mode particles
2 and greater LW absorption. This disparity highlights the sensitivity of climatic effects to the
3 specified aerosol size distribution. On a separate note, Ferraro et al (2011) neglected to alter
4 the aerosol density component in the calculation of their aerosol masses and specific
5 optical properties [A. Ferraro, personal communication]. The density that they used for
6 all the aerosols of 1000 kg/m^3 is arguably applicable to black carbon, but not to sulfate
7 and titania (which instead are ~ 1600 and $\sim 4000 \text{ kg/m}^3$). Therefore, their aerosol burdens
8 for sulfate and titania should be multiplied by 1.6 and 4 respectively, and their optical
9 coefficients divided by 1.6 and 4, to obtain appropriate values.

10 It is important to note that the climate impacts described in section 4 above are dependent on
11 the optical properties of the aerosol, which are further dependent on the aerosol particle's
12 size, shape, and composition [e.g. Kravitz et al., 2012]. In this investigation, the dry-mode
13 size distribution of the aerosol species is held constant, and hygroscopic growth is not
14 represented in the BC and titania schemes, nor are the effects of internal mixing represented.
15 Observations have shown that fresh BC aerosol is predominantly hydrophobic, but the
16 uptake of soluble particulates (e.g. secondary organics) results in increased
17 hygroscopicity [Liu et al., 2013]. Mineral dust, which contains 1-10% titania by mass
18 [Ndour et al., 2008], exhibits low hygroscopicity for radii $< 0.1 \mu\text{m}$ and similar growth
19 to equivalently-sized sulfate aerosol thereafter [Koehler et al., 2009]. Although the
20 historical stratospheric water vapor content is low ($\sim 4.2 \text{ ppmv}$ in the tropical lower
21 stratosphere during the HIST period), aerosol-induced stratospheric warming in the TTL
22 would increase the specific humidity of air entering the stratosphere, therefore impacting
23 hygroscopic growth. The injection of aerosol into pre-existing aerosol layers would lead to
24 larger particles through coagulation and condensation, which would further ~~alters~~ alter the
25 aerosol's optical and physical properties. The actual size of the aerosol in an SAI scheme
26 would therefore depend on the injection strategy (e.g. location/ season) and the size and
27 composition of the injected species [e.g. Carslaw and Kärcher, 2006; Heckendorn et al.,
28 2009]. Recent research from Heckendorn et al (2009), Pierce et al (2010), English et al
29 (2012), and Weisenstein et al (2015) have highlighted the importance of representing aerosol
30 growth in SAI simulations. A detailed assessment of the aerosol microphysics for sulfate, BC,
31 and titania injection is not within the scope of this paper, but presents an important subject for
32 future work.

1 The climatic impacts described in section 4 are specific to geoengineering against a
2 baseline RCP8.5 scenario. If instead we had used a middle-of-the-road GHG-
3 concentrations scenario such as RCP4.5 [Taylor et al., 2012], as used in the first tier of
4 GeoMIP scenarios [Kravitz et al., 2011], then less aerosol-injection would be needed to
5 obtain TOA-Imb=0 and therefore the aerosol deposition rates and atmospheric mass
6 concentrations would be less than those reported in section 4. One would expect that the
7 magnitude of stratospheric temperature changes (Fig. 8) and therefore zonal-mean zonal
8 wind changes (Fig. 12) would be much less for each of the aerosols, possibly
9 confounding the conclusions giving here relating to their comparative efficacy. An
10 estimate for the amount of SAI required for RCP4.5 can be garnered from integrating the
11 temperature anomalies for RCP8.5 and RCP4.5 for the period 2020-2100. The ratio of
12 the integrated temperature anomalies for RCP4.5 to RCP8.5 is 0.43, hence we can
13 assume that the injection rates required for RCP4.5 are ~0.43 of those for RCP8.5,
14 producing a climate perturbation ~0.43 times as great. A further set of simulations,
15 which instead utilise RCP4.5 as the baseline scenario, would be required to test this
16 hypothesis.

17 We have used prescribed ozone fields in these simulations because representing stratospheric
18 chemistry is prohibitively computationally expensive for the multiple centennial simulations
19 performed here [The HadGEM2 development team, 2011]. Kravitz et al (2012) showed that
20 BC injection could potentially result in global ozone depletion of >50%, therefore the
21 chemistry changes in SAI could potentially exceed the importance of the physical changes in
22 terms of climatic impacts (e.g. UV radiation at the surface). Tilmes et al (2012) showed that
23 SW-scattering by geoengineered sulfate could potentially compensate for ozone-loss by back-
24 scattering UV radiation in the tropics, but that this effect was insufficiently compensatory at
25 high latitudes. Their result was scenario-dependent; ozone loss due to heterogeneous
26 chemistry is enhanced for smaller particles and in the presence of higher free-radical
27 concentrations. Therefore, additional research is needed in order to understand the effects on
28 atmospheric chemistry of injecting alternative aerosols. This work has already been started
29 for titania by Tang et al (2014).

30 Another important aspect of SAI which is comparatively under-researched is the potential for
31 impacts on human health. Aerosol concentrations in the air near the surface are of interest
32 because of potential human respiratory impacts [Robock, 2008]. For instance, the USA's
33 National Institute for Occupational Safety and Health (NIOSH) recommends a maximum

1 exposure limits of 0.3 mg/m^3 for ultrafine titania particles (radius $<0.05 \text{ }\mu\text{m}$ and 2.4 mg m^{-3}
2 for fine particles (radius $< 1.5 \text{ }\mu\text{m}$) [Dankovic et al., 2011]. After undergoing coagulation
3 and ageing in the atmosphere, it is likely that the second exposure limit is more
4 applicable to this work. In our simulations, the maximum 2090's near-surface air
5 concentration of titania (e.g. Fig. 4) for land regions between 60°S - 60°N is 254 ng/m^3 , which
6 is of the order of ~~10^2~~ 10^3 less than the NIOSH 'fine-particle' exposure limit. The equivalent
7 maximum concentration anomalies of BC in ~~G3BC~~-geoBC and SO_4 in ~~G3S~~-geoSulf are 10
8 ng/m^3 and 1851 ng/m^3 respectively. More work is needed to assess the potential impacts of
9 SAI on air quality and human health.

10 Another thus far unmentioned aspect of this research is the potential for surface albedo
11 modification by aerosol deposition. In particular, BC deposition on snow reduces the snow
12 albedo through enhanced snow-melt and the coarsening of snow grains, which results in
13 amplified high-latitude warming [Marks and King, 2013]. HadGEM2-CCS does not include
14 the BC-on-snow feedback; therefore we estimate it by comparing the deposition rates for
15 2090s ~~G3BC~~-geoBC with the historical period. Jiao et al (2014) report that the simulated
16 annual mean Arctic ($>60^\circ\text{N}$) BC deposition for the 2006-2009 period ranges from $13\text{-}35 \times 10^7$
17 kg/yr for the AEROCOM Phase II models. The annual mean Arctic BC deposition for the
18 2006-2009 period from our HadGEM2-CCS simulations is $23 \times 10^7 \text{ kg/yr}$, which is within the
19 AEROCOM range. The annual mean Arctic BC deposition anomaly for the 2090s period in
20 ~~G3BC~~-geoBC is $19.6 \times 10^7 \text{ kg/yr}$. Therefore, the effects of dirty snow in such an SAI scenario
21 would likely be significant, which would have impacts on the distribution of temperature,
22 particularly at high latitudes, potentially confounding some of our conclusions.

23 This research has highlighted potential climate impacts of injecting various stratospheric
24 aerosols in order to ameliorate global warming. However, further research is needed to
25 further assess the climatic impacts of stratospheric aerosol injection such as the impacts on
26 ozone. Whilst research ~~has shown~~ indicates that SAI ~~to be~~ capable of averting certain
27 climate changes such as surface-warming, SAI provides no amelioration for other climate
28 impacts, such as ocean acidification. It is therefore important to note that the safest possible
29 solution to avoiding the sort of climate change instantiated by (e.g.) Fig. 6a of this report is to
30 effectively mitigate greenhouse-gas emissions.

31

1 **Author contribution**

2 ACJ designed the experiments, performed the simulations, analysed the data, and wrote the
3 manuscript with guidance and advice from JMH and AJ.

4 **Data sets**

5 Data used to generate figures, graphs, plots and tables are freely available via contacting the
6 lead author: aj247@exeter.ac.uk.

7 **Acknowledgements**

8 The authors would like to thank Valentina Aquila for supplying AVHRR and SAGE data,
9 and to Peter Cox, Angus Ferraro, David Keith and Alan Robock for helpful discussions. We
10 also thank 2 anonymous reviewers and John Dykema for their comments and suggestions.
11 ACJ was supported by a Met Office/NERC CASE (ref. 580009183) PhD studentship; JMH
12 and AJ were supported by the Joint UK DECC/Defra Met Office Hadley Centre Climate
13 Programme (GA01101).

14

15

16

1 *References*

- 2 d'Almeida, G. A., Koepke, P., and Shettle, E. P.: Atmospheric aerosols: global climatology
3 and radiative characteristics, A. Deepak Publishing, Hampton, USA, 1991.
- 4 Aquila, V., Oman, L. D., Stolarski, R. S., Colarco, P. R., and Newman, P. A.: Dispersion of
5 the volcanic sulfate cloud from a Mount Pinatubo-like eruption, *J. Geophys. Res.*, 117,
6 D06216, doi:10.1029/2011JD016968., 2012.
- 7 Aquila, V., Garfinkel, C. I., Newman, P. A., Oman, L. D., and Waugh, D. W.: Modifications
8 of the quasi-biennial oscillation by a geoengineering perturbation of the stratospheric aerosol
9 layer, *Geophys. Res. Lett.*, 41, 1738–1744, doi:10.1002/2013GL058818., 2014.
- 10 Bala, G., Duffy, P. B., and Taylor, K. E.: Impact of geoengineering schemes on the global
11 hydrological cycle, *P. Natl. Acad. Sci. USA.*, June 3 2008, vol. 105, no. 22, 7664-7669, 2008.
- 12 Baldwin, M. P., Gray, L. J., Dunkerton, T. J., Hamilton, K., Haynes, P. H., Randel, W. J.,
13 Holton, J. R., Alexander, M. J., Hirota, I., Horinouchi, T., Jones, D. B. A., Kinnersley, J. S.,
14 Marquardt, C., Sato, K., and Takahashi, M.: The quasi-biennial oscillation, *Rev. Geophys.*,
15 39(2), 179–229, doi:10.1029/1999RG000073., 2001.
- 16 [Bellouin, N., Boucher, O., Haywood, J., Johnson, C., Jones, A., Rae, J., and Woodward, S.:](#)
17 [Improved representation of aerosols for HadGEM2, Hadley Centre technical note 73, Hadley](#)
18 [Centre, Met Office, Exeter, UK, 42pp., available at](#)
19 http://www.metoffice.gov.uk/media/pdf/8/f/HCTN_73.pdf (last accessed 01/16), 2007.
- 20 Bellouin, N., Rae, J., Johnson, C., Haywood, J., Jones, A., and Boucher, O.: Aerosol forcing
21 in the Hadley Centre CMIP5 simulations by HadGEM2-ES and the role of ammonium
22 nitrate, *J. Geophys. Res.*, 116, D20206, doi:10.1029/2011JD016074, 2011.
- 23 Berdahl, M., Robock, A., Ji, D., Moore, J. C., Jones, A., Kravitz, B., and Watanabe, S.:
24 Arctic cryosphere response in the Geoengineering Model Intercomparison Project G3 and G4
25 scenarios, *J. Geophys. Res. Atmos.*, 119, 1308–1321, doi:10.1002/2013JD020627., 2014.
- 26 Carslaw, K. C., and Kärcher, B.: Stratospheric aerosol processes, in *Assessment of*
27 *Stratospheric Aerosol Properties*, edited by L. Thomason and T. Peter, WCRP 124,
28 WMO/TD 1295, SPARC Rep. 4, World. Meteorol. Organ., Geneva, Switzerland, 2006.

- 1 Collins, M., Knutti, R., Arblaster, J., Dufresne, J.-L., Fichet, T., Friedlingstein, P., Gao, X.,
2 Gutowski, W. J., Johns, T., Krinner, G., Shongwe, M., Tebaldi, C., Weaver, A. J., and
3 Wehner, M.: Long-term Climate Change: Projections, Commitments and Irreversibility. In:
4 Climate Change 2013: The Physical Science Basis. Contribution of Working Group I to the
5 Fifth Assessment Report of the Intergovernmental Panel on Climate Change [Stocker, T.F.,
6 Qin, D., Plattner, G.-K., Tignor, M., Allen, S. K., Boschung, J., Nauels, A., Xia, Y., Bex, V.,
7 and Midgley, P.M. (eds.)]. Cambridge University Press, Cambridge, United Kingdom and
8 New York, NY, USA., 2013.
- 9 Crutzen, P.: Albedo Enhancement by Stratospheric Sulfur Injections: A Contribution to
10 Resolve a Policy Dilemma?, *Climatic Change*, August 2006, Volume 77, Issue 3, pp 211-
11 220, 2006.
- 12 Dankovic, D., Kuempel, E., Geraci, C., Gilbert, S., Rice, F., Schulte, P., Smith, R.,
13 Sofge, C., Wheeler, M., Lentz, T. J., Zumwalde, R., Maynard, A., Attfield, M., Pinheiro,
14 G., Ruder, A., Hubbs, A., Ahlers, H., Lynch, D., Toraason, M., and Vallyathan, V.:
15 Current intelligence bulletin 63: occupational exposure to titanium dioxide., Cincinnati,
16 OH: U.S. Department of Health and Human Services, Public Health Service, Centers for
17 Disease Control and Prevention, National Institute for Occupational Safety and Health,
18 DHHS (NIOSH) Publication No. 2011-160, 2011 Apr; :1-119, 2011.
- 19 [Davies, T., Cullen, M. J. P., Malcolm, A. J., Mawson, M. H., Staniforth, A., White, A. A.,](#)
20 [and Wood, N.: A new dynamical core for the Met Office's global and regional modelling of](#)
21 [the atmosphere. *Q. J. R. Meteorol. Soc.*, 131, pp. 1759–1782. doi: 10.1256/qj.04.101. 2005](#)
- 22 Deepak, A., and Gerber, H. E. (Eds.): Report of the experts meeting on aerosols and their
23 climatic effects (Williamsburg, Virginia, March 1983), Rep. WCP-55, World Clim.
24 Programme, World Meteorol. Organ., Geneva, 1983.
- 25 [Dessler, A. E., Schoeberl, M. R., Wang, T., Davis, S. M., and Rosenlof, K. H.: Stratospheric](#)
26 [water vapor feedback, *Proc. Natl. Acad. Sci. U.S.A.*, 110, 45, 18087-18091, doi:](#)
27 [10.1073/pnas.1310344110, 2013.](#)
- 28 [Dhomse, S. S., Emmerson, K. M., Mann, G. W., Bellouin, N., Carslaw, K. S., Chipperfield,](#)
29 [M. P., Hommel, R., Abraham, N. L., Telford, P., Braesicke, P., Dalvi, M., Johnson, C. E.,](#)
30 [O'Connor, F., Morgenstern, O., Pyle, J. A., Deshler, T., Zawodny, J. M., and Thomason, L.](#)
31 [W.: Aerosol microphysics simulations of the Mt.~Pinatubo eruption with the UM-UKCA](#)

Formatted: Line spacing: 1.5 lines

- 1 [composition-climate model, Atmos. Chem. Phys., 14, 11221-11246, doi:10.5194/acp-14-](#)
2 [11221-2014, 2014.](#)
- 3 Deshler, T., and Anderson-Sprecher, R.: Non-volcanic stratospheric aerosol trends: 1971–
4 2004, in Assessment of Stratospheric Aerosol Properties, edited by L. Thomason and T.
5 Peter, WCRP 124, WMO/TD 1295, SPARC Rep. 4, World Meteorolo. Organ., Geneva,
6 Switzerland, 2006.
- 7 Driscoll, S., Bozzo, A., Gray, L. J., Robock, A., and Stenchikov, G.: Coupled Model
8 Intercomparison Project 5 (CMIP5) simulations of climate following volcanic eruptions, J.
9 Geophys. Res. Atmos., 117, D17105, doi:10.1029/2012JD017607, 2012.
- 10 [L'Ecuyer, T. S., Beaudoin, H. K., Rodell, M., Olson, W., Lin, B., Kato, S., Clayson, C. A.,](#)
11 [Wood, E., Sheffield, J., Adler, R., Huffman, G., Bosilovich, M., Gu, G., Robertson, F.,](#)
12 [Houser, P. R., Chambers, D., Famiglietti, J. S., Fetzer, E., Liu, W. T., Gao, X., Schlosser, C.](#)
13 [A., Clark, E., Lettenmaier, D. P., and Hilburn, K.: The Observed State of the Energy Budget](#)
14 [in the Early Twenty-First Century. J. Climate, 28, 8319–8346.,](#)
15 [doi:http://dx.doi.org/10.1175/JCLI-D-14-00556.1](http://dx.doi.org/10.1175/JCLI-D-14-00556.1), 2015.
- 16 English, J. M., Toon, O. B., and Mills, M. J.: Microphysical simulations of sulfur burdens
17 from stratospheric sulfur geoengineering, Atmos. Chem. Phys., 12, 4775–4793,
18 doi:10.5194/acp-12-4775-2012, 2012.
- 19 Ferraro, A. J., Highwood, E. J., and Charlton-Perez, A. J.: Stratospheric heating by
20 potential geoengineering aerosols, Geophys. Res. Lett., 38, L24706,
21 doi:10.1029/2011GL049761., 2011.
- 22 Ferraro, A. J., Highwood, E. J., and Charlton-Perez, A. J.: Weakened tropical circulation
23 and reduced precipitation in response to geoengineering, Environ. Res. Lett., 9, 014001,
24 2014.
- 25 Forster, P., Ramaswamy, V., Artaxo, P., Berntsen, T., Betts, R., Fahey, D. W., Haywood,
26 J., Lean, J., Lowe, D. C., Myhre, G., Nganga, J., Prinn, R., Raga, G., Schulz, M., and
27 Van Dorland, R.: Changes in Atmospheric Constituents and in Radiative Forcing. In:
28 Climate Change 2007: The Physical Science Basis. Contribution of Working Group I to
29 the Fourth Assessment Report of the Intergovernmental Panel on Climate Change
30 [Solomon, S., Qin, D., Manning, M., Chen, Z., Marquis, M., Averyt, K. B., Tignor, M.,

- 1 and Miller, H. L. (eds.)). Cambridge University Press, Cambridge, United Kingdom and
2 New York, NY, USA., 2007.
- 3 [Gettelman, A., Hegglin, M. I., Son, S.-W., Kim, J., Fujiwara, M., Birner, T., Kremser, S., Rex,](#)
4 [M., Añel, J. A., Akiyoshi, H., Austin, J., Bekki, S., Braesike, P., Brühl, C., Butchart, N.,](#)
5 [Chipperfield, M., Dameris, M., Dhomse, S., Garny, H., Hardiman, S. C., Jöckel, P., Kinnison,](#)
6 [D. E., Lamarque, J. F., Mancini, E., Marchand, M., Michou, M., Morgenstern, O., Pawson,](#)
7 [S., Pitari, G., Plummer, D., Pyle, J. A., Rozanov, E., Scinocca, J., Shepherd, T. G., Shibata,](#)
8 [K., Smale, D., Teyssède, H., and Tian, W.: Multimodel assessment of the upper troposphere](#)
9 [and lower stratosphere: Tropics and global trends, *J. Geophys. Res.*, 115, D00M08,](#)
10 [doi:10.1029/2009JD013638, 2010.](#)
- 11 The HadGEM2 Development Team: Martin, G. M., Bellouin, N., Collins, W. J., Culverwell,
12 I. D., Halloran, P.R., Hardiman, S. C., Hinton, T. J., Jones, C. D., McDonald, R. E., McLaren,
13 A. J., O'Connor, F. M., Roberts, M. J., Rodriguez, J. M., Woodward, S., Best, M. J., Brooks,
14 M. E., Brown, A. R., Butchart, N., Dearden, C., Derbyshire, S. H., Dharssi, I., Doutriaux-
15 Boucher, M., Edwards, J. M., Falloon, P. D., Gedney, N., Gray, L. J., Hewitt, H. T., Hobson,
16 M., Huddleston, M. R., Hughes, J., Ineson, S., Ingram, W. J., James, P. M., Johns, T. C.,
17 Johnson, C. E., Jones, A., Jones, C. P., Joshi, M. M., Keen, A. B., Liddicoat, S., Lock, A. P.,
18 Maidens, A. V., Manners, J. C., Milton, S. F., Rae, J. G. L., Ridley, J. K., Sellar, A., Senior,
19 C. A., Totterdell, I. J., Verhoef, A., Vidale, P. L., and Wiltshire, A.: The HadGEM2 family of
20 Met Office Unified Model climate configurations, *Geosci. Model Dev.*, 4, 723–757,
21 [www.geosci-model-dev.net/4/723/2011/](#), doi:10.5194/gmd-4-723-2011, 2011.
- 22 Haywood, J.M., Jones, A., Clarisse, L., Bourassa, A., Barnes, J., Telford, P., Bellouin N.,
23 Boucher, O., Agnew, P., Clerbaux, C., Coheur, P., Degenstein, D., and Braesicke, P.:
24 Observations of the eruption of the Sarychev volcano and simulations using the HadGEM2
25 climate model, *J. Geophys. Res.*, 115, D21212, doi:10.1029/2010JD014447, 2010.
- 26 [Haywood, J. M., Bellouin, N., Jones, A., Boucher, O., Wild, M., and Shine, K. P.: The roles](#)
27 [of aerosol, water vapor and cloud in future global dimming/brightening, *J. Geophys. Res.*,](#)
28 [116, D20203, doi:10.1029/2011JD016000., 2011.](#)
- 29 Haywood, J.M., Jones, A., Bellouin, N., and Stephenson, D.: Asymmetric forcing from
30 stratospheric aerosols impacts Sahelian rainfall, [Nat. Clim. Change](#), 3, 660–
31 665, doi:10.1038/nclimate1857, 2013.

- 1 Heckendorn, P., Weisenstein, D., Fueglistaler, S., Luo, B. P., Rozanov, E., Schraner, M.,
2 Thomason, L. W., and Peter, T.: The impact of geoengineering aerosols on stratospheric
3 temperature and ozone, *Environ. Res. Lett.*, 4, 045108, doi:10.1088/1748-9326/4/4/045108,
4 2009.
- 5 [Illingworth, A. J., Barker, H. W., Beljaars, A., Ceccaldi, M., Chepfer, H., Clerbaux, N., Cole,](#)
6 [J., Delanoë, J., Domenech, C., Donovan, D. P., Fukuda, S., Hiraoka, M., Hogan, R. J.,](#)
7 [Huenerbein, A., Kollias, P., Kubota, T., Nakajima, T., Nakajima, T. Y., Nishizawa, T., Ohno,](#)
8 [Y., Okamoto, H., Oki, R., Sato, K., Satoh, M., Shephard, M. W., Velázquez-Blázquez, A.,](#)
9 [Wandinger, U., Wehr, T., and van Zadelhoff, G.-J.: The EarthCARE Satellite: The Next Step](#)
10 [Forward in Global Measurements of Clouds, Aerosols, Precipitation, and Radiation, *Bull.*](#)
11 [Amer. Meteor. Soc.](#), 96, 1311–1332. doi: <http://dx.doi.org/10.1175/BAMS-D-12-00227.1>,
12 [2015.](#)
- 13 International Civil Aviation Organisation (ICAO): Manual of the ICAO Standard
14 Atmosphere: extended to 80 kilometres (262 200 feet), Doc 7488/3, Third ed., 1993
- 15 Jiao, C., Flanner, M. G., Balkanski, Y., Bauer, S. E., Bellouin, N., Bernsten, T. K., Bian,
16 H., Carslaw, K. S., Chin, M., De Luca, N., Diehl, T., Ghan, S. J., Iversen, T., Kirkevåg,
17 A., Koch, D., Liu, X., Mann, G. W., Penner, J. E., Pitari, G., Schulz, M., Seland, Ø.,
18 Skeie, R. B., Steenrod, S. D., Stier, P., Takemura, T., Tsigaridis, K., van Noije, T., Yun,
19 Y., and Zhang, K.: An AeroCom assessment of black carbon in Arctic snow and sea ice,
20 *Atmos. Chem. Phys.*, 14, 2399–2417, doi:10.5194/acp-14-2399-2014, 2014.
- 21 Kawatani, Y., and Hamilton, K.: Weakened stratospheric quasi-biennial oscillation driven by
22 increased tropical mean upwelling, *Nature*, 497, 478–481, doi:10.1038/nature12140, 2013.
- 23 Kharin, V. V., Zwiers, F. W., Zhang, X., and Wehner, M.: Changes in temperature and
24 precipitation extremes in the CMIP5 ensemble, *Climatic Change* (2013) 119:345–357,
25 DOI 10.1007/s10584-013-0705-8, 2013.
- 26 [Koehler, K. A., Kreidenweis, S. M., DeMott, P. J., Petters, M. D., Prenni, A. J., and Carrico,](#)
27 [C. M.: Hygroscopicity and cloud droplet activation of mineral dust aerosol, *Geophys. Res.*](#)
28 [Lett.](#), 36, L08805, doi:10.1029/2009GL037348.. 2009.

- 1 Kravitz, B., Robock, A., Boucher, O., Schmidt, H., Taylor, K. E., Stenchikov, G., and Schulz,
2 M.: The Geoengineering Model Intercomparison Project (GeoMIP). *Atmosph. Sci. Lett.*, 12:
3 162–167. doi: 10.1002/asl.316, 2011.
- 4 Kravitz, B., Robock, A., Shindell, D. T., and Miller, M. A.: Sensitivity of stratospheric
5 geoengineering with black carbon to aerosol size and altitude of injection, *J. Geophys.*
6 *Res.*, 117, D09203, doi:10.1029/2011JD017341., 2012.
- 7 Kravitz, B., Robock, A., Forster, P. M., Haywood, J. M., Lawrence, M. G., and Schmidt, H.:
8 An overview of the Geoengineering Model Intercomparison Project (GeoMIP), *J. Geophys.*
9 *Res. Atmos.*, 118, 13,103–13,107, doi:10.1002/2013JD020569, 2013.
- 10 [Kravitz, B., Robock, A., Tilmes, S., Boucher, O., English, J. M., Irvine, P. J., Jones, A.,](#)
11 [Lawrence, M. G., MacCracken, M., Muri, H., Moore, J. C., Niemeier, U., Phipps, S. J.,](#)
12 [Sillmann, J., Storelvmo, T., Wang, H., and Watanabe, S.: The Geoengineering Model](#)
13 [Intercomparison Project Phase 6 \(GeoMIP6\): simulation design and preliminary results,](#)
14 [Geosci. Model Dev., 8, 3379-3392, doi:10.5194/gmd-8-3379-2015, 2015.](#)
- 15 [Liu, D., Allan, J., Whitehead, J., Young, D., Flynn, M., Coe, H., McFiggans, G., Fleming, Z.](#)
16 [L., and Bandy, B.: Ambient black carbon particle hygroscopic properties controlled by](#)
17 [mixing state and composition, *Atmos. Chem. Phys.*, 13, 2015-2029, doi:10.5194/acp-13-](#)
18 [2015-2013, 2013.](#)
- 19 Lombardo, K., Colle, B. A., and Zhang, Z.: Evaluation of Historical and Future Cool
20 Season Precipitation over the Eastern United States and Western Atlantic Storm Track
21 Using CMIP5 Models. *J. Climate*, 28, 451–467., doi: http://dx.doi.org/10.1175/JCLI-D-
22 14-00343.1, 2015.
- 23 [MacMartin, D.G., Keith, D.W., Kravitz, B., and Caldeira, K.: Management of trade-offs](#)
24 [in geoengineering through optimal choice of non-uniform radiative forcing, *Nat. Clim.*](#)
25 [Change, 3, 365-368, doi:10.1038/nclimate1722, 2013.](#)
- 26 Marks, A. A., and King, M. D.: The effect of snow/sea ice type on the response of albedo
27 and light penetration depth (e-folding depth) to increasing black carbon, *The Cryosphere*,
28 8, 1625–1638, www.the-cryosphere.net/8/1625/2014/, doi:10.5194/tc-8-1625-2014,
29 2014.

Formatted: Line spacing: 1.5 lines

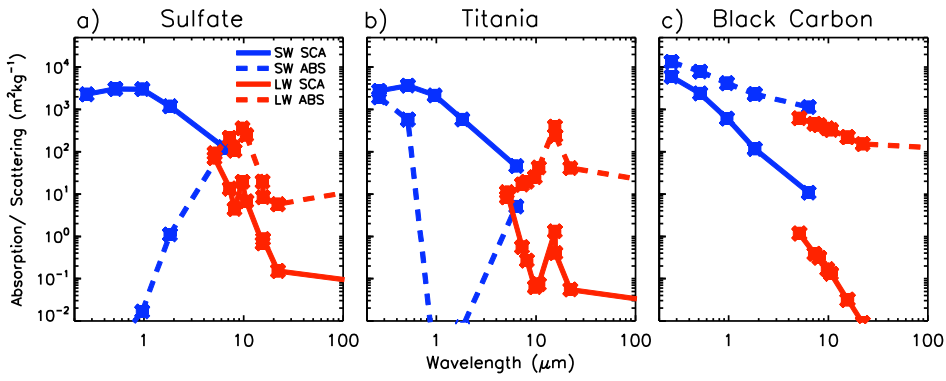
- 1 Meinshausen, M., Smith, S. J., Calvin, K. V., Daniel, J. S., Kainuma, M. L. T., Lamarque, J.-
2 F., Matsumoto, K., Montzka, S. A., Raper, S. C. B., Riahi, K., Thomson, A. M., Velders, G.
3 J. M., and Vuuren, D. Van.: "The RCP Greenhouse Gas Concentrations and their Extension
4 from 1765 to 2300." *Climatic Change* (Special Issue), DOI: 10.1007/s10584-011-0156-z,
5 2011.
- 6 [Ndour, M., D'Anna, B., George, C., Ka, O., Balkanski, Y., Kleffmann, J., Stemmler, K., and
7 Ammann, M.: Photoenhanced uptake of NO₂ on mineral dust: Laboratory experiments and
8 model simulations, *Geophys. Res. Lett.*, 35, L05812, doi:10.1029/2007GL032006., 2008.](#)
- 9 Niemeier, U., Schmidt, H., and Timmreck, C.: The dependency of geoengineered
10 sulfate aerosol on the emission strategy, *Atmos. Sci. Lett.*, 12, 189–194, doi:10.1002/asl.304,
11 2011.
- 12 [Niemeier, U., Schmidt, H., Alterskjær, K., and Kristjánsson, J. E.: Solar irradiance reduction
13 via climate engineering: Impact of different techniques on the energy balance and the
14 hydrological cycle, *J. Geophys. Res. Atmos.*, 118, 11,905–11, 917,
15 doi:10.1002/2013JD020445., 2013.](#)
- 16 Oman, L., Robock, A., Stenchikov, G. L. & Thordarson, T.: High-latitude eruptions cast
17 shadow over the African monsoon and the flow of the Nile., *Geophys. Res. Lett.*, 33, L18711
18 16, 2006.
- 19 [Peters, G. P., Andrew, R. M., Boden, T., Canadell, J. G., Ciais, P., Le Quéré, C., Marland, G.,
20 Raupach, M. R., and Wilson, C.: The challenge to keep global warming below 2 °C, *Nat.
21 Clim. Change*, 3, 4-6, doi:10.1038/nclimate1783, 2013](#)
- 22 Pierce, J. R., D. K. Weisenstein, P. Heckendorn, T. Peter, and D. W. Keith (2010), Efficient
23 formation of stratospheric aerosol for climate engineering by emission of condensable vapor
24 from aircraft, *Geophys. Res. Lett.*, 37, L18805, doi:10.1029/2010GL043975.
- 25 Pitari, G., Aquila, V., Kravitz, B., Robock, A., Watanabe, S., Cionni, I., De Luca, N., Di
26 Genova, G., Mancini, E., and Tilmes, S.: Stratospheric ozone response to sulfate
27 geoengineering: Results from the Geoengineering Model Intercomparison Project (GeoMIP),
28 *J. Geophys. Res. Atmos.*, 119, 2629–2653, doi:10.1002/2013JD020566., 2014.
- 29 [Pithan, F., and Mauritsen, T.: Arctic amplification dominated by temperature feedbacks in
30 contemporary climate models, *Nat. Geosci.*, 7, 181-184, doi:10.1038/ngeo2071, 2014.](#)

- 1 Pope, F. D., Braesicke, P., Grainger, R. G., Kalberer, M., Watson, I. M., Davidson, P. J., and
2 Cox, R. A.: Stratospheric aerosol particles and solar-radiation management, *Nature Climate*
3 *Change*, 2, 713–719, doi:10.1038/nclimate1528, 2012.
- 4 [Priestley, K. J., Smith, G. L., Thomas, S., Cooper, D., Lee III, R. B., Walikainen, D., Hess,](#)
5 [P., Szewczyk, Z. P., and Wilson, R.: Radiometric Performance of the CERES Earth Radiation](#)
6 [Budget Climate Record Sensors on the EOS Aqua and Terra Spacecraft through April 2007,](#)
7 [J. Atmos. Oceanic Technol.](#), 28, 3–21, doi: <http://dx.doi.org/10.1175/2010JTECHA1521.1>,
8 [2011.](#)
- 9 Pruppacher, H.R., and Klett, J.D.: *Microphysics of Clouds and Precipitation*, D. Reidel
10 Publishing Company, Dordrecht, ISBN: 978-90-277-1106-9, Holland, Reprinted 1980.
- 11 [Ramaswamy, V., Boucher, O., Haigh, J., Hauglustaine, D., Haywood, J., Myhre, G.,](#)
12 [Nakajima, T., Shi, G. Y. and Solomon S.: Radiative forcing of climate change. In:](#)
13 [Climate Change 2001: The Scientific Basis. Contribution of Working Group I to the](#)
14 [Third Assessment Report of the Intergovernmental Panel on Climate Change \[Houghton,](#)
15 [J.T., et al. \(eds.\)\]. Cambridge University Press, Cambridge, United Kingdom and New](#)
16 [York, NY, USA, pp. 349–416., 2001.](#)
- 17 Rasch, P. J., Tilmes, S., Turco, R. P., Robock, A., Oman, L., Chen, C.-C., Stenchikov, G. L.,
18 and Garcia, R. R.: An overview of geoengineering of climate using stratospheric sulphate
19 aerosols, *Phil. Trans. R. Soc. A* 2008 366 4007–4037; DOI: 10.1098/rsta.2008.0131, 2008.
- 20 Ribarsky, M. W.: Titanium dioxide, in *Handbook of Optical Constants of Solids*, edited by E.
21 Palik, pp. 795–804, Academic, Orlando, Fla, 1985.
- 22 Robock, A., Oman, L., and Stenchikov, G. L.: Regional climate responses to geoengineering
23 with tropical and Arctic SO₂ injections. *J. Geophys. Res.* 113, D16101
24 doi:10.1029/2008JD010050., 2008.
- 25 [Schmidt, H., Rast, S., Bunzel, F., Esch, M., Giorgetta, M., Kinne, S., Krismer, T.,](#)
26 [Stenchikov, G., Timmreck, S., Tomassini, L., and Walz, M.: Response of the middle](#)
27 [atmosphere to anthropogenic and natural forcings in the CMIP5 simulations with the Max](#)
28 [Planck Institute Earth system model, J. Adv. Model. Earth Syst.](#), 5, 98–116,
29 [doi:10.1002/jame.2001](http://dx.doi.org/10.1002/jame.2001), 2013.

- 1 Schoeberl, M. R., Douglass, A. R., Stolarski, R. S., Pawson, S., Strahan, S. E., and Read, W.:
- 2 Comparison of lower stratospheric tropical mean vertical velocities, *J. Geophys. Res.*, 113,
- 3 D24109, doi:10.1029/2008JD010221., 2008.
- 4 [von Schuckmann, K., Palmer, M.D., Trenberth, K.E., Cazenave, A., Chambers, D.,](#)
- 5 [Champollion, N., Hansen, J., Josey, S.A., Loeb, N., Mathieu, P.-P., Meyssignac, B., and](#)
- 6 [Wild, M.: An imperative to monitor Earth's energy imbalance, *Nat. Clim. Change*, 6, 138–](#)
- 7 [144, doi:10.1038/nclimate2876, 2016.](#)
- 8 Shepherd, J., et al.: *Geoengineering the climate: Science, governance, and uncertainty*. Royal
- 9 Society Policy document 10/09, 82 pp, ISBN: 978-0-85403-773-5, 2009.
- 10 Stenchikov, G., Robock, A., Ramaswamy, V., Schwarzkopf, M. D., Hamilton, K., and
- 11 Ramachandran, S.: Arctic Oscillation response to the 1991 Mount Pinatubo eruption: Effects
- 12 of volcanic aerosols and ozone depletion, *J. Geophys. Res.*, 107(D24), 4803,
- 13 doi:10.1029/2002JD002090, 2002.
- 14 [Tang, M. J., Telford, P. J., Pope, F. D., Rkiouak, L., Abraham, N. L., Archibald, A. T.,](#)
- 15 [Braesicke, P., Pyle, J. A., McGregor, J., Watson, I. M., Cox, R. A., and Kalberer, M.:](#)
- 16 [Heterogeneous reaction of N₂O₅ with airborne TiO₂ particles and its implication for](#)
- 17 [stratospheric particle injection, *Atmos. Chem. Phys.*, 14, 6035-6048, doi:10.5194/acp-14-](#)
- 18 [6035-2014, 2014.](#)
- 19 Taylor, K. E., Stouffer, R. J., and Meehl, G. A.: An Overview of CMIP5 and the Experiment
- 20 Design, *Bull. Amer. Meteor. Soc.*, 93, 485–498, doi: <http://dx.doi.org/10.1175/BAMS-D-11->
- 21 [00094.1](http://dx.doi.org/10.1175/BAMS-D-11-00094.1), 2012.
- 22 Tegtmeier, S., Kruger, K., Wohltmann, I., Schoellhammer, K., and Rex, M.: Variations
- 23 of the residual circulation in the Northern Hemispheric winter, *J. Geophys. Res.*, 113,
- 24 D16109, doi:10.1029/2007JD009518., 2008.
- 25 Teller, E., Wood, L., and Hyde, R.: *Global Warming and Ice Ages: I. Prospects for Physics-*
- 26 *Based Modulation of Global Change*, Lawrence Livermore National Laboratory Publication
- 27 UCRL-JC-128715, 18 pp., 1997.

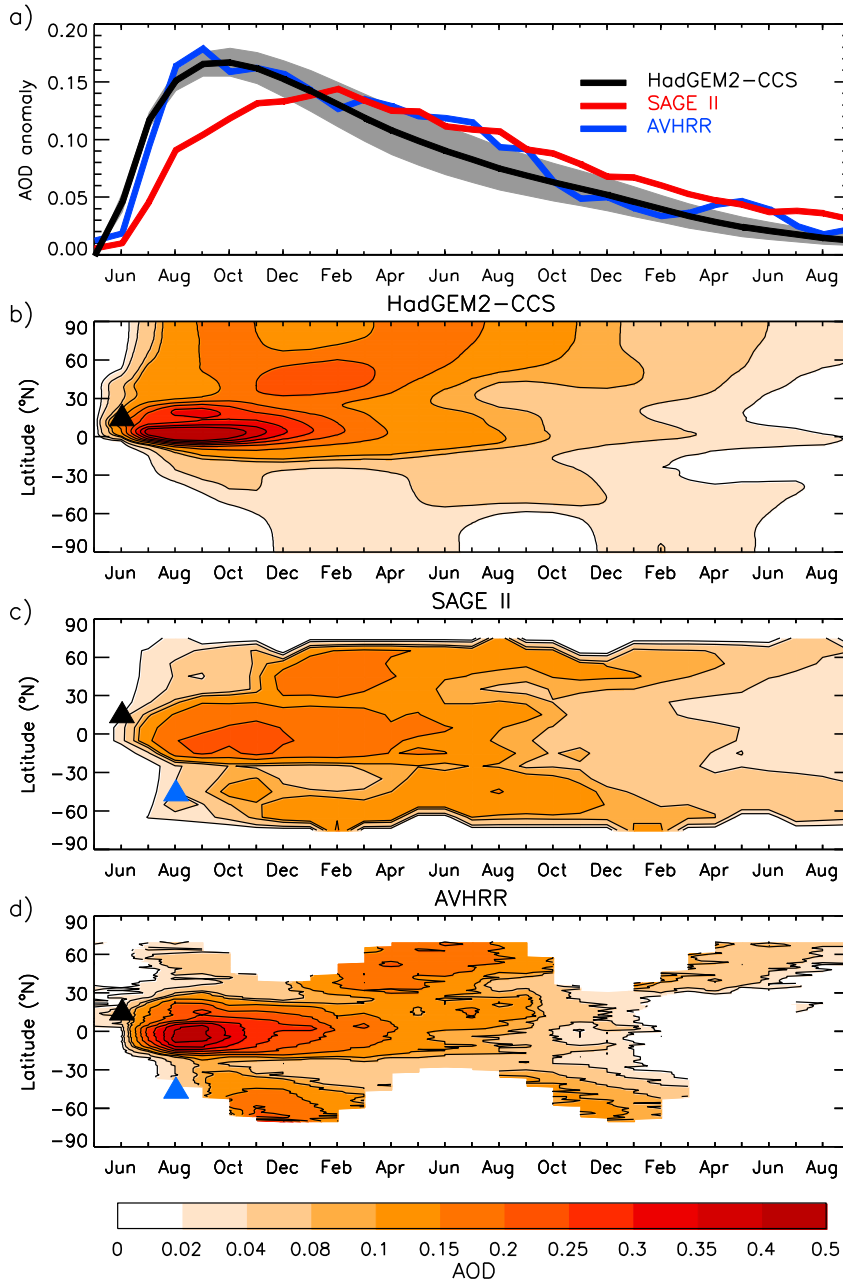
- 1 Tilmes, S., Garcia, R. R., Kinnison, D. E., Gettelman, A., and Rasch, P. J.: Impact of
2 geoengineered aerosols on the troposphere and stratosphere, *J. Geophys. Res.*, 114, D12305,
3 doi:10.1029/2008JD011420, 2009.
- 4 Tilmes, S., Kinnison, D. E., Garcia, R. R., Salawitch, R., Canty, T., Lee-Taylor, J.,
5 Madronich, S., and Chance, K.: Impact of very short-lived halogens on stratospheric ozone
6 abundance and UV radiation in a geo-engineered atmosphere, *Atmos. Chem. Phys.*, 12,
7 10945-10955, doi:10.5194/acp-12-10945-2012, 2012.
- 8 Tilmes, S., Fasullo, J., Lamarque, J.-F., Marsh, D. R., Mills, M., Alterskjær, K., Muri, H.,
9 Kristjánsson, J. E., Boucher, O., Schulz, M., Cole, J. N. S., Curry, C. L., Jones, A., Haywood,
10 J., Irvine, P. J., Ji, D., Moore, J. C., Karam, D. B., Kravitz, B., Rasch, P. J., Singh, C., Yoon,
11 J.-H., Niemeier, U., Schmidt, H., Robock, A., Yang, S., and Watanabe, S.: The hydrological
12 impact of geoengineering in the Geoengineering Model Intercomparison Project (GeoMIP), *J.*
13 *Geophys. Res. Atmos.*, 118, 11,036–11,058, doi:10.1002/jgrd.50868., 2013.
- 14 ~~Weisenstein, D. K., and Keith, D. W.: Solar geoengineering using solid aerosol in the~~
15 ~~stratosphere, *Atmos. Chem. Phys. Discuss.*, 15, 11799–11851, 2015.~~
- 16 Weisenstein, D. K., Keith, D. W., and Dykema, J. A.: Solar geoengineering using solid
17 aerosol in the stratosphere, *Atmos. Chem. Phys.*, 15, 11835-11859, doi:10.5194/acp-15-
18 11835-2015, 2015.
- 19 Yang, H., Zhu, S., and Pan, N.: Studying the Mechanisms of Titanium Dioxide as Ultraviolet-
20 Blocking Additive for Films and Fabrics by an Improved Scheme, *Journal of Applied*
21 *Polymer Science*, Vol. 92, 3201–3210, 2004.
- 22 Yu, X., Moore, J. C., Cui, X., Rinke, A., Ji, D., Kravitz, B., and Yoon, J.-H.: Impacts,
23 effectiveness and regional inequalities of the GeoMIP G1 to G4 solar radiation
24 management scenarios, *Global and Planetary Change*, 129, 10–22,
25 <http://dx.doi.org/10.1016/j.gloplacha.2015.02.010>, 2015.
- 26

1

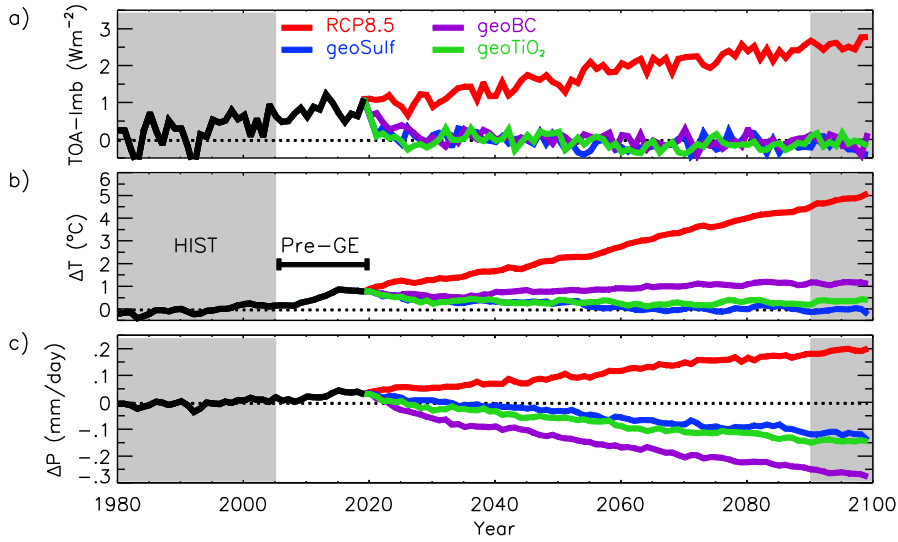


2

3 **Figure 1.** Optical properties as a function of wavelength for a) accumulation-mode
4 sulfate, b) titania, c) black carbon. Points are plotted at the middle of each spectral
5 waveband, [as detailed in Bellouin et al \(2007\)](#)
6

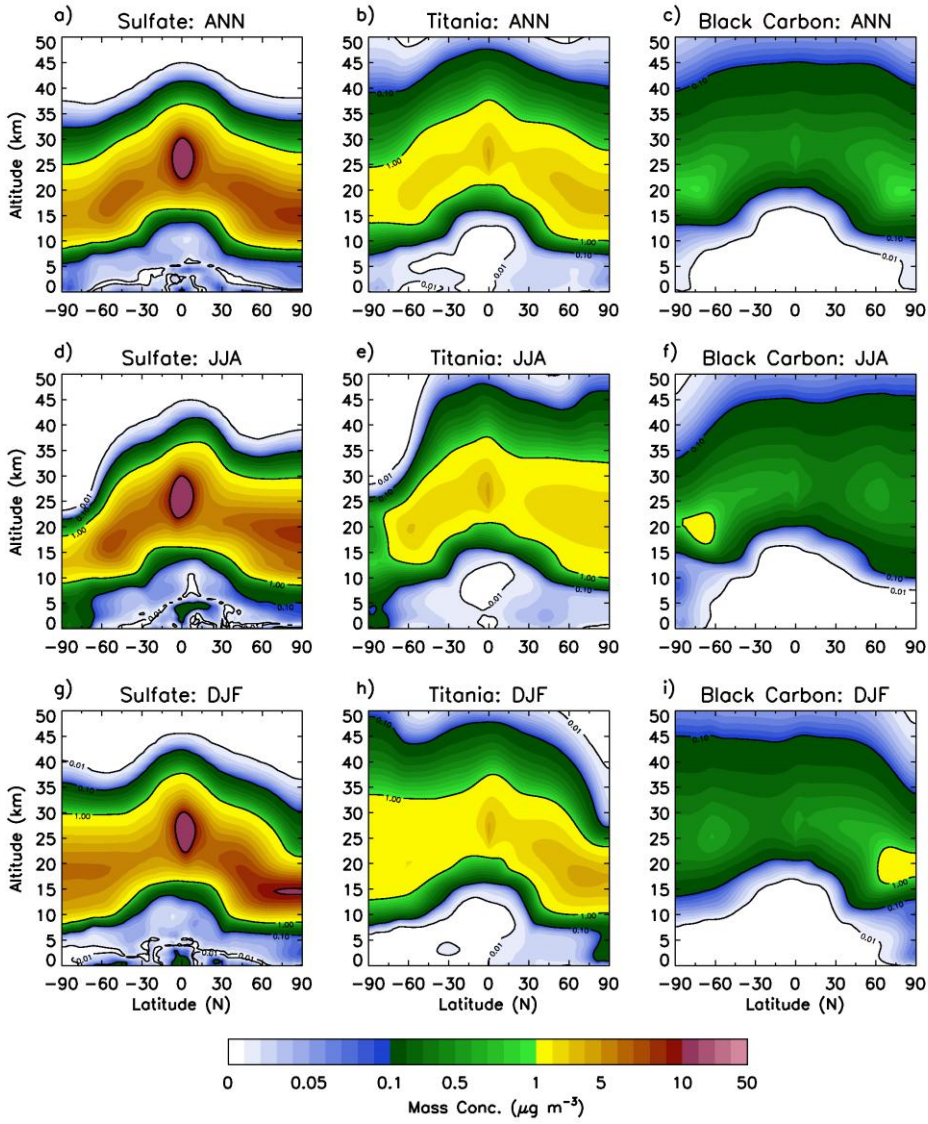


1
 2 **Figure 2.** a) 75°S-75°N-mean 550nm sulfate AOD anomaly for the Pinatubo simulations and
 3 observations, b-d) timeseries of zonal-mean 550nm sulfate AOD anomaly



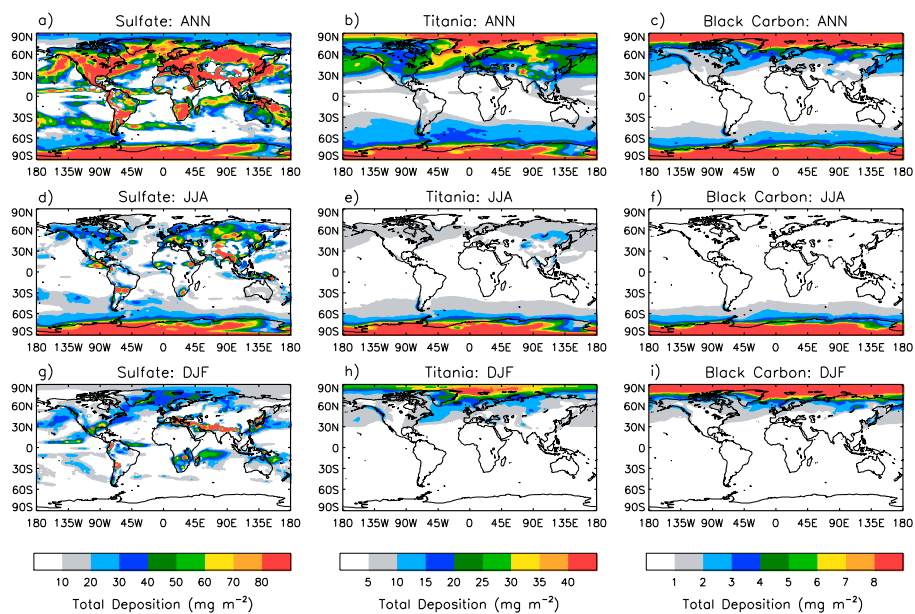
1
2
3
4
5

Figure 3. Timeseries of annual/global-mean a) top-of-the-atmosphere radiative flux anomaly with respect to the pre-industrial control simulation b) near-surface air temperature anomaly with respect to the HIST period c) global mean precipitation anomaly with respect to HIST



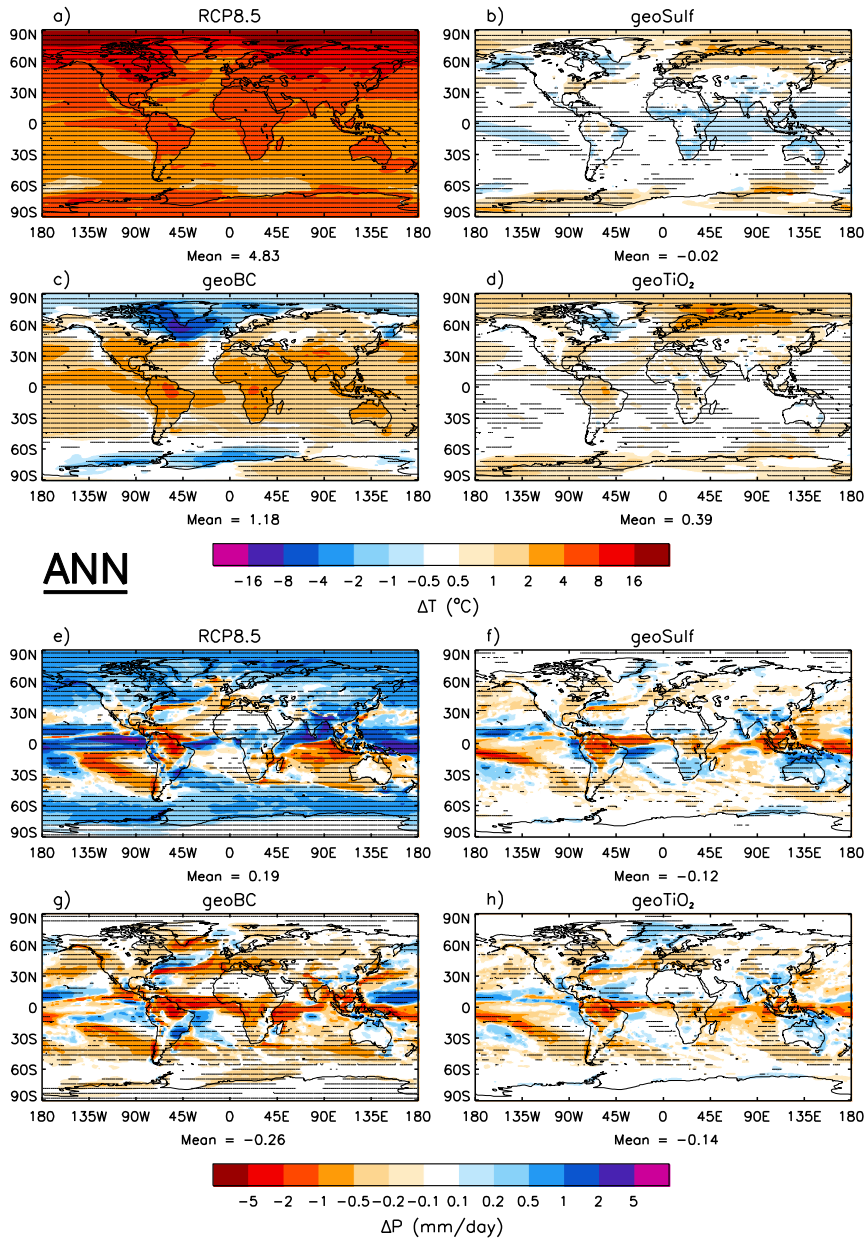
1
2
3
4

Figure 4. Annual and seasonal zonal-mean mass concentration anomalies for sulfate (*geoSulf* - left), titania (*geoTiO₂* - centre) and black carbon (*geoBC* - right)



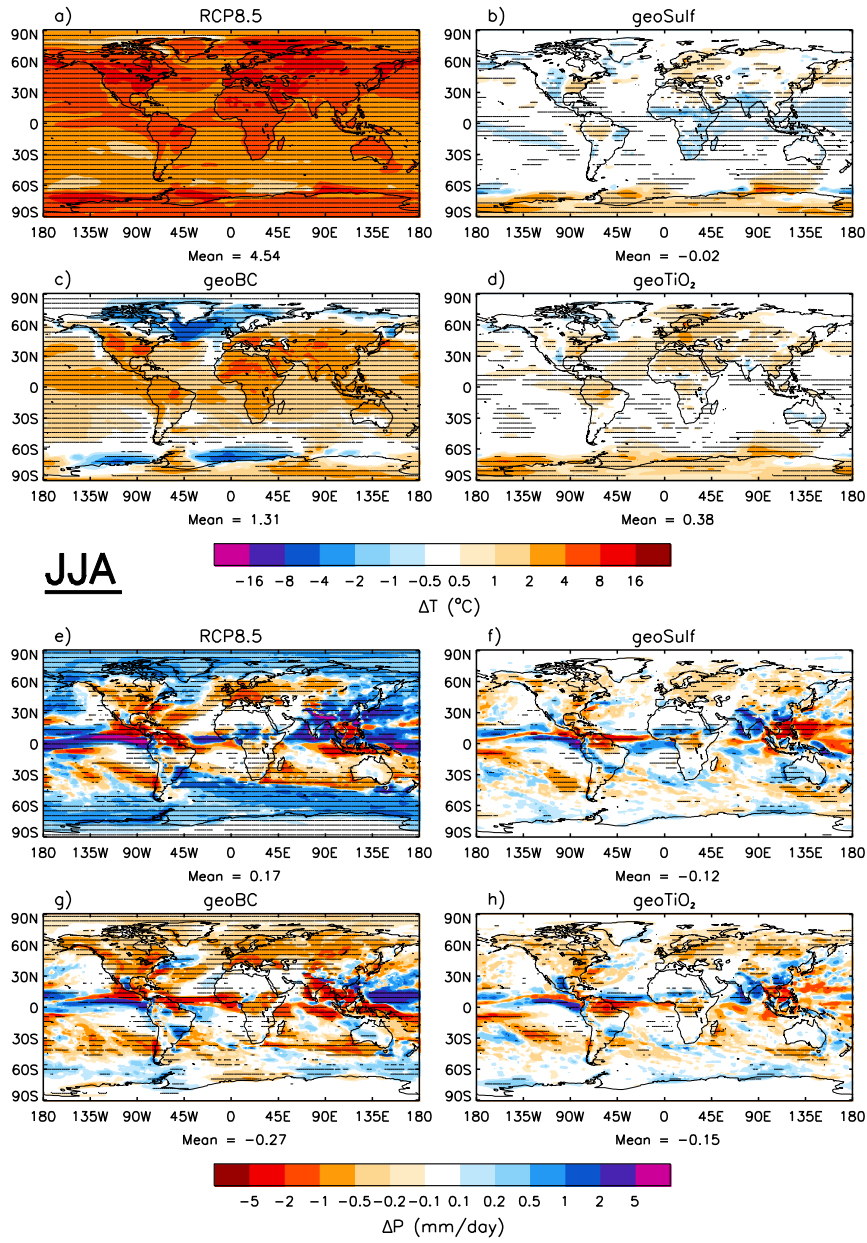
1
2
3
4
5

Figure 5. Annual and seasonal total deposition anomalies (in units of $\text{mg m}^{-2} \text{yr}^{-1}$ and $0.25 \times \text{mg m}^{-2} \text{yr}^{-1}$ respectively)



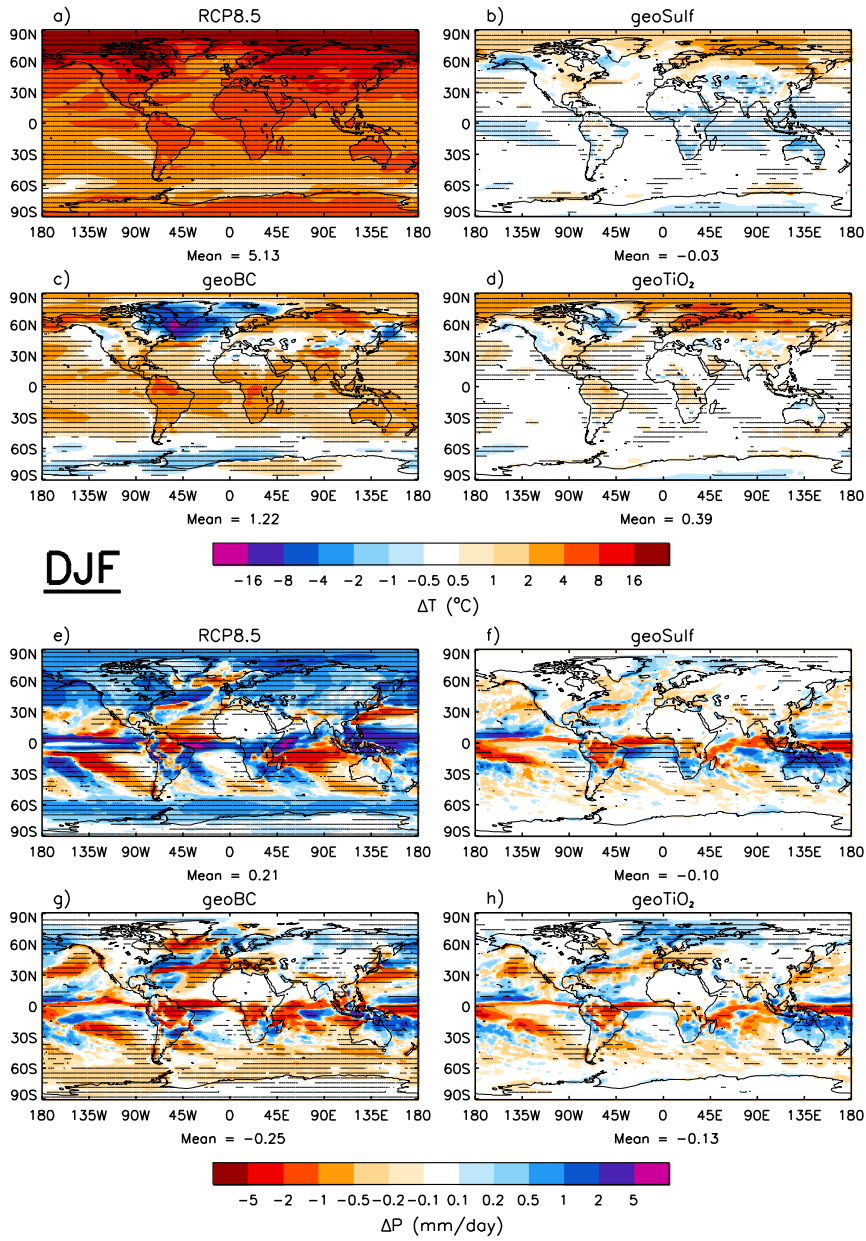
1

2 **Figure 6.** Annual-mean near-surface air temperature (top) and precipitation rate (bottom)
 3 anomalies with respect to HIST. Stippling indicates where changes are significant at the 5%
 4 level using a two-tailed Student's *t*-test



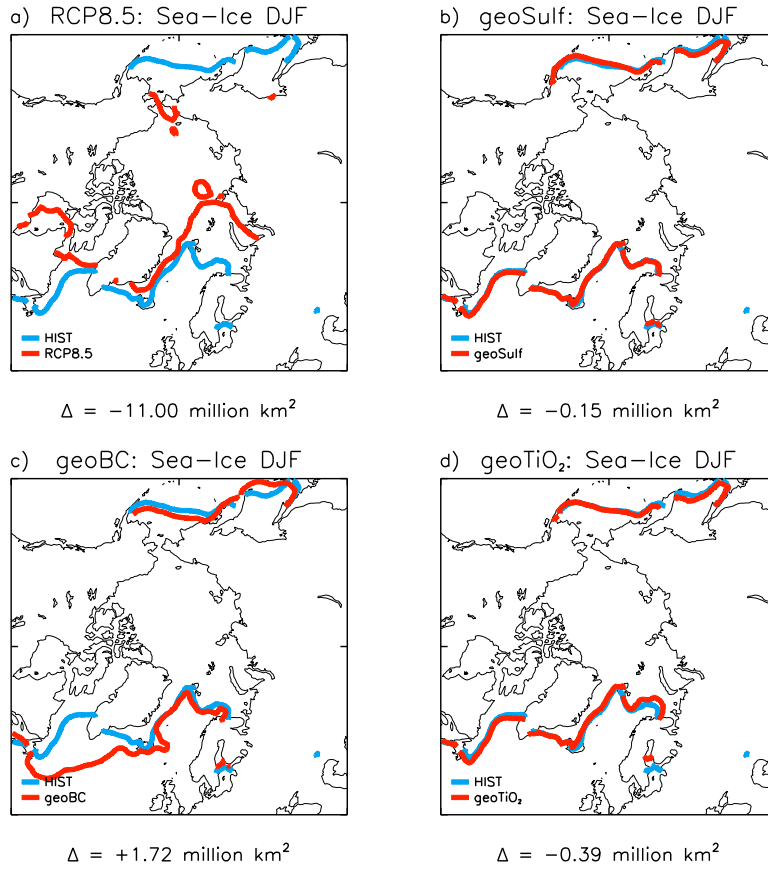
1
2
3
4

Figure 7. JJA near-surface air temperature (top) and precipitation rate (bottom) anomalies with respect to HIST



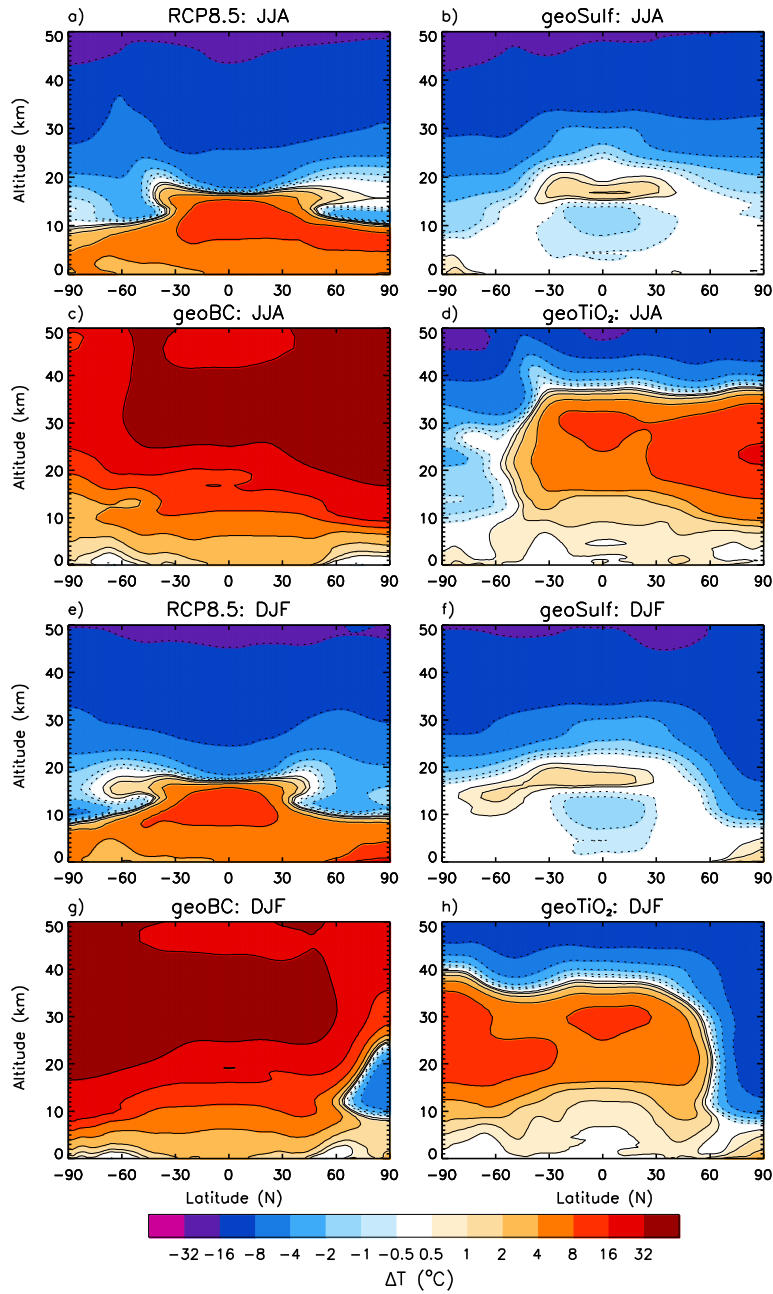
1
2
3
4

Figure 8. DJF near-surface air temperature (top) and precipitation rate (bottom) anomalies with respect to HIST



1
2
3

Figure 9. DJF northern-hemisphere sea-ice edge plotted with the HIST extent

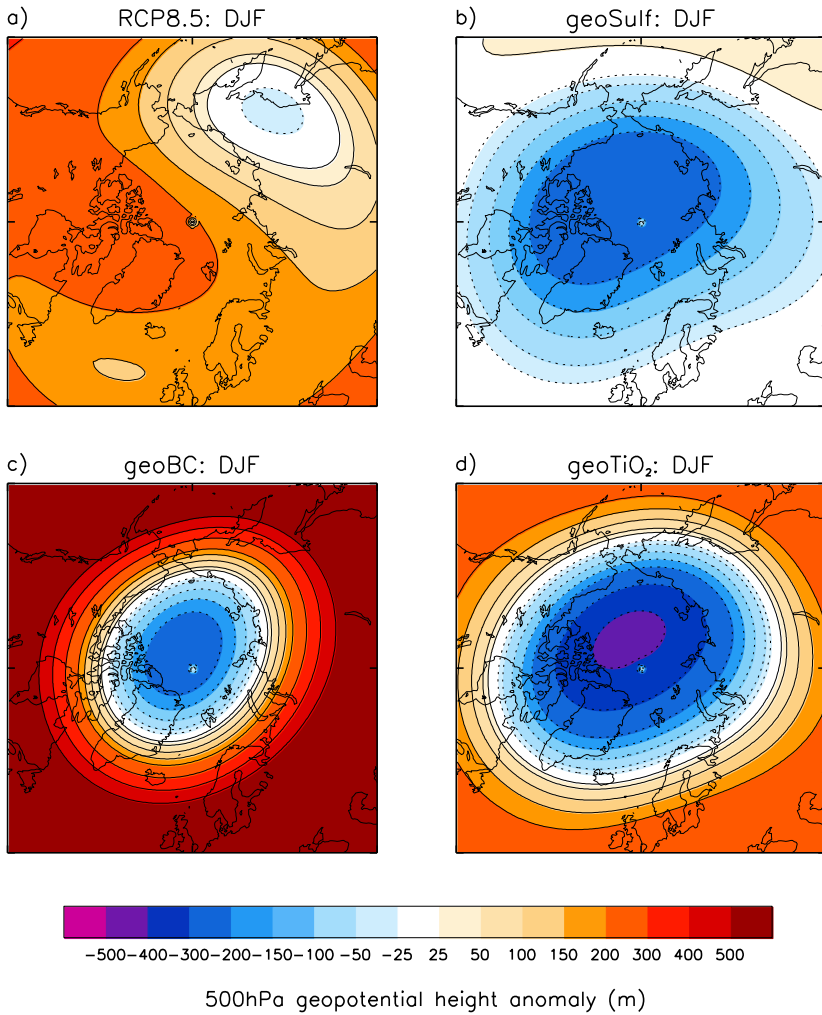


1

2

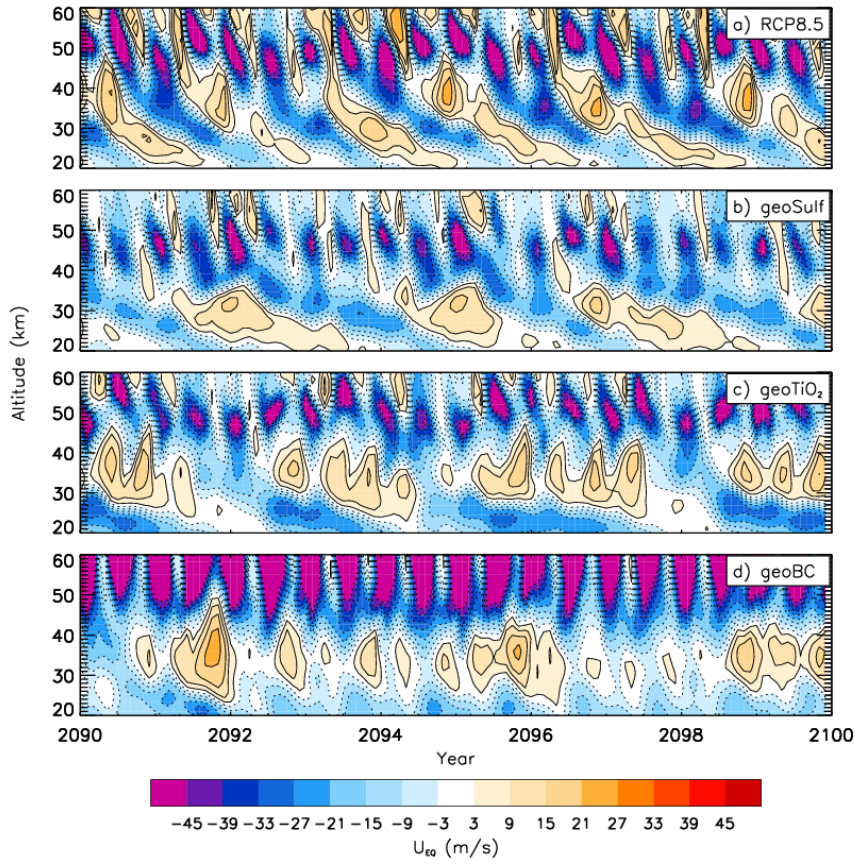
3

Figure 10. JJA (top) and DJF (bottom) zonal-mean temperature anomaly with altitude, with respect to HIST



1
2
3
4

Figure 11. *DJF 50hPa geopotential height anomaly*



1
2
3
4
5
6
7

Figure 12. Timeseries of equatorial (5°S-5°N) zonal-mean zonal wind profile